

Turing instability and 2-D pattern formation in reaction-diffusion systems derived from kinetic theory

Stefano Boccelli¹, Giorgio Martalò², Romina Travaglini^{3,4*}

¹Planetary Magnetospheres Laboratory, NASA Goddard Space Flight Center

8800 Greenbelt rd, Greenbelt, MD 20771, USA

stefano.boccelli@nasa.gov

²Dipartimento di Matematica "Felice Casorati", Università di Pavia

Via Ferrata 5, 27100, Pavia, Italy

giorgio.martalo@unipv.it

³INDAM – Istituto Nazionale di Alta Matematica "Francesco Severi"

Piazzale Aldo Moro 5, 00185, Roma, Italy

⁴Dipartimento di Scienze Matematiche, Fisiche e Informatiche, Università di Parma

Parco Area delle Scienze 53/A, I-43124, Parma, Italy

romina.travaglini@unipr.it

* corresponding author

Abstract

We investigate Turing instability and pattern formation in two-dimensional domains for two reaction-diffusion models, obtained as diffusive limits of kinetic equations for mixtures of monatomic and polyatomic gases. The first model is of Brusselator type, which, compared with the classical formulation, presents an additional parameter whose role in stability and pattern formation is discussed. In the second framework, the system exhibits standard nonlinear diffusion terms typical of predator-prey models, but differs in reactive terms. In both cases, the kinetic-based approach proves effective in relating macroscopic parameters, often set empirically, to microscopic interaction mechanisms, thereby rigorously identifying admissible parameter ranges for the physical description. Furthermore, weakly nonlinear analysis and numerical simulations extend previously known one-dimensional results and reveal a wider scenario of spatial structures, including spots, stripes, and hexagonal arrays, that better reflect the richness observed in real-world systems.

Keywords: Reaction-diffusion equations, Kinetic theory, Weakly Nonlinear Analysis, Pattern formation,

MSC Classification: 35K57, 35Q92, 82C40

1 Introduction

Reaction-diffusion equations play a crucial role in various areas of applied sciences, offering a powerful framework for modeling diverse spatio-temporal dynamics in complex systems, that involve both interactions among the components and diffusive phenomena. Since the pioneering work of Alan Turing in 1952 [38], who first demonstrated how diffusion could destabilize a uniform equilibrium and lead to the emergence of stationary patterns, many reaction-diffusion models have been formulated at the macroscopic level by specifying partial differential equations for the concentrations or densities of interacting species.

Diffusion coefficients and reaction rates are introduced or fitted through phenomenological considerations. A well-known example is the Brusselator model, a classical autocatalytic reaction-diffusion system developed by Prigogine and collaborators [22, 33]. It has been extensively studied for its capacity to generate stable spatial patterns and to exhibit Turing instability under suitable parameter regimes [16, 32]. Moving forward, these models have been applied to a wide range of phenomena across disciplines. Examples include morphogenesis in autocatalytic chemical reactions [16, 32], vegetation patterns in arid landscapes [1, 14], epidemic spread [2, 15], lesion formation in autoimmune dynamics [6, 17], and even socioeconomic processes such as market dynamics and migration [3].

Beyond their broad applicability, classical reaction-diffusion systems possess a well developed mathematical theory explaining how patterns emerge from uniform states. In the two-species activator-inhibitor framework introduced by Turing [38] and extensively applied to biological systems in [30], diffusion-driven instability occurs when a homogeneous steady state, stable in the absence of diffusion, becomes unstable once diffusion is included, typically requiring a strong disparity between diffusion coefficients. Near the instability threshold, the dominant spatial modes select characteristic wavelengths, and in two-dimensional domains these modes can interact to produce a variety of stationary structures, including stripes, spots, labyrinthine patterns, and hexagonal arrays, as demonstrated numerically in early works like [29] and experimentally in chemical systems (e.g., [40]).

While one-dimensional settings allow only simple periodic configurations, two dimensions enable mode resonances, symmetry-breaking interactions, and the coexistence or competition of multiple pattern analyzed in depth through bifurcation and weakly nonlinear theory [20]. Weakly nonlinear (amplitude-equation) analysis has been a central tool for understanding this pattern-selection mechanism, for predicting the stability of different morphologies, and for developing more systematic criteria for spot-stripe selection and related transitions, as explored for instance in [25].

These classical approaches have proven highly successful in reproducing observed patterns across many domains, nevertheless, they often do not account for the underlying microscopic interactions between individual particles, agents, or molecules. As a result, the macroscopic parameters, such as diffusion coefficients and reaction constants, may lack a

clear mechanistic interpretation. This limits the model's predictive power, particularly in contexts where one seeks to relate observed macroscopic phenomena to their underlying physical or chemical processes.

In contrast, one can formulate macroscopic reaction–diffusion models directly from a microscopic description. This strategy allows the fundamental microscopic phenomena of interest to be modeled explicitly, with the macroscopic equations arising only afterward as collective effects of the microscopic dynamics. In doing so, the need to assign empirical parameter values is reduced or eliminated; instead, the resulting macroscopic expressions are grounded in the underlying microscopic physics of the problem.

To this aim, extended kinetic theory offers a powerful multiscale methodology, which has been employed in a variety of physical, chemical, and biological problems through the years (see for example [4, 12, 28, 37]). By starting from a mesoscopic description of particle interactions, it is possible to rigorously derive macroscopic reaction–diffusion systems through suitable hydrodynamic limits. These tools have been widely used in different frameworks, from classical Boltzmann theory of gas dynamics [5, 8, 21] to the models of cells and tissues (see e.g. [11] and references therein). Similarly, the micro-macro connection has been investigated in the case when the reactive collision operators are phenomenological models, such as Fokker-Planck or BGK [34, 35, 36], or for discrete velocity models [41].

This approach not only provides explicit expressions for macroscopic parameters in terms of microscopic quantities but also reveals how collective behavior emerges from individual interactions. For the sake of completeness, it is important to remark that, from a broader perspective, kinetic theory offers the possibility of working across multiple scales, ultimately leading to a deeper understanding of collective phenomena and allowing, for example, insight into how a population is distributed around the mean value. Some steps in this direction have recently been taken in [10, 26].

In this paper, we focus on two such reaction-diffusion systems [8, 27], recently derived from kinetic models of gas mixtures involving monatomic and polyatomic species in proper multiple scale regimes. These models consider a mixture of interacting gases, initially modeled at the microscopic level using kinetic equations. From the microscopic formulation, the authors subsequently obtain a macroscopic formulation in the form of a reaction-diffusion system of equations. Unlike classical reaction–diffusion systems where diffusion and reaction rates are free parameters, the models derived in [8, 27] inherit nonlinear and cross-diffusion structures that arise directly from collision dynamics at the microscopic scale, leading to constraints and couplings absent in phenomenological models.

Specifically, these references show how linear and nonlinear diffusion terms can be obtained through a rigorous limit of Boltzmann-like kinetic equations. More precisely, in the continuum limit, in [8] components densities are governed by a Brusselator-type description, where a further parameter appears in addition to those present in the classic model for autocatalytic reactions; whereas, in [27] a model with nonlinear cross diffusion is derived, reproducing the diffusive terms of [13] but differing from it in the reactive contributions. In both cases, the parameters in the macroscopic setting can be expressed in terms of the microscopic quantities, such as mass, internal energy and collision frequency , allowing for a physically grounded parameter selection and a deeper understanding of pattern forma-

tion mechanisms.

In the study of macroscopic reaction-diffusion systems, considerable attention is devoted to Turing instability, which represents a key mechanism for the emergence of spatio-temporal patterns. Specifically, Turing instability refers to the process by which a stable stationary solution becomes destabilized in the presence of diffusion, leading to the formation of stable non-uniform structures. This issue has been addressed in both [8, 27], where macroscopic coefficients are explicitly linked to microscopic parameters, showing that system properties such as stability and the onset of Turing instability depend on the internal energy levels of monoatomic and polyatomic species. In those works, both the analysis and the numerical investigation were carried out in one-dimensional domains.

Moving from one-dimensional analysis to a two-dimensional framework is essential, as it enables the emergence of richer and more complex spatial patterns – such as spots, stripes, and hexagonal arrays – that cannot appear in one dimension. Moreover, extending to two-dimensional models brings simulations closer to the spatial complexity observed in real-world systems.

The aim of this paper is twofold: first, to revisit the derivation from kinetic equations in order to highlight how the dependence on microscopic dynamics naturally imposes constraints on the choice of parameters; second, to analyze the phenomenon of Turing instability and pattern formation in two-dimensional domains for varying parameters within the validity range. The latter objective involves the study of interactions between multiple modes and wavevectors, which give rise to a more intricate landscape of possible instabilities and transitions.

This can be addressed through a weakly nonlinear analysis [31], which allows us to predict the emergence and stability of different spatial configurations. Such an approach, which is widely used in describing the formation of two dimensional patterns in various fields ad cellular biology [7], population dynamics [24] or vegetation-water interplay [14], has been extensively explored for Brusselator-type models [16, 32, 39] in the context of chemical reactions. Here, we extend this investigation by considering, on the one hand, the model for mono/polyatomic gas mixtures, which introduces an additional coefficient, and on the other hand, by applying the same methodology, the model in [27].

In both cases, as in the basic Turing instability analysis, we are able to derive conditions on the microscopic parameters that give rise to a variety of two-dimensional scenarios.

The paper is organized as follows: we briefly recall the derivation of the two models as diffusive limit of proper kinetic equations in Section 2. The Turing instability and the pattern formation for the Brusselator-type model and the description with cross diffusion are discussed in Section 3 and 4, respectively: the emergence of non-uniform stable solutions is investigated through weakly nonlinear analysis, and confirmed and extended numerically. Some concluding remarks are given in Section 5.

2 Kinetic equations and diffusive limits

We recall here the physical setting used in [8, 27] to derive some reaction-diffusion systems as diffusive limit of kinetic equations in gas dynamics.

We first provide some preliminaries on the physical modeling adopted here to describe interacting mixtures of polyatomic species [18, 19]. Each gas species, say C^i , may have a number l^i of possible discrete values for the internal energy. We denote each one of these values by E_j^i , $j = 1, \dots, l^i$. As a consequence, we treat the i -th species as composed by l^i components C_j^i , $j = 1, \dots, l^i$, being the component C_j^i characterized by the internal energy E_j^i . We report here a general encounter expressed as follows

$$C_j^i + C_k^h \rightleftharpoons C_m^l + C_p^n. \quad (2.1)$$

In the case of mechanical collisions, in which molecules do not change their nature, we may have elastic scattering, when there is not energy dissipation due to absorption by the particles, and in the formulation (2.1) we have $(i, j) = (l, m)$ and $(h, k) = (n, p)$. If, instead, there is a variation of the internal energies of the pair of impinging particles, we have the collision (2.1) with $i = l$ and $h = n$, but $j \neq m$ and/or $k \neq p$. Finally, in case of chemical encounters, there is also a mass transfer and particles change the gas species they belong to. When this happens we have collision (2.1) with $(i, h) \neq (l, n)$ and $i \neq n$. Indicating by $f_j^i(t, \mathbf{x}, \mathbf{v})$ the distribution function associated to the component C_j^i depending on time t , position \mathbf{x} , and molecular velocity \mathbf{v} , the Boltzmann-type operator for encounter (2.1) takes the following form (dependence on time and space is omitted)

$$\begin{aligned} \mathcal{Q}_i^{XX}(f_j^i, f_k^h, f_m^l, f_p^n) = & \int_{\mathbb{R}^3} \int_{\mathbb{S}^2} \mathcal{H}(g^2 - \delta_{ih}^{ln}) g \sigma(g, \hat{\Omega} \cdot \hat{\Omega}') \\ & \times \left[\left(\frac{m_i m_h}{m_l m_n} \right)^3 f_m^l(\mathbf{v}') f_p^n(\mathbf{w}') - f_j^i(\mathbf{v}) f_k^h(\mathbf{w}) \right] d\mathbf{w} d\hat{\Omega}', \end{aligned} \quad (2.2)$$

where

- (\mathbf{v}, \mathbf{w}) are the ingoing microscopic velocities of particles with mass m_i and m_h , respectively;
- $(\mathbf{v}', \mathbf{w}')$ are the post interaction microscopic velocities of particles having mass m_l and m_n ($l = i$ and $n = h$ in mechanical encounters);
- the heaviside function \mathcal{H} depends on the modulus of relative velocity $\mathbf{g} = \mathbf{v} - \mathbf{w}$ and on the energy gap $\delta_{ih}^{ln} = 2m_i m_h (E_m^l + E_p^n - E_j^i - E_k^h)/(m_i + m_h)$ (the gap is null in elastic collisions);
- the cross sections σ depends on the modulus of the ingoing relative velocity and on the deflection angle $\hat{\Omega} \cdot \hat{\Omega}'$, being $\hat{\Omega}$ the direction of vector \mathbf{g} .

The gaseous mixture considered in [8, 27] is composed by two constituents diffusing in a host medium. The first constituent Y is assumed to be polyatomic with two different energy levels E_1 and E_2 ; therefore, it can be split in two components Y_1 and Y_2 . The second gas Z is supposed to be monatomic, endowed with a unique energy level E_Z . We indicate by m_Y and m_Z the masses of polyatomic and monatomic gas particles, respectively.

The background medium is a mixture whose gases are much denser than the previous ones. We suppose that this mixture is composed by three components A , B and C , with masses m_A , m_B and m_C . We assume that their distributions are Maxwellian functions with unit temperature and zero mean velocity

$$f_i = n_i \mathcal{M}_i(\mathbf{v}), \quad \mathcal{M}_i(\mathbf{v}) = n_i \left(\frac{m_i}{2\pi} \right)^{3/2} \exp \left(-\frac{m_i |\mathbf{v}|^2}{2} \right), \quad (2.3)$$

$i = A, B, C$; the number densities n_i are supposed to be constant.

The evolution of the distribution functions f_1 , f_2 and f_Z of constituents Y_1 , Y_2 and Y_Z is governed by Boltzmann-like equations, where the collision operator takes account of elastic, inelastic and reactive interactions. More precisely, in addition to elastic collisions, the following transitions occur



The kinetic equation for f_i ($i = 1, 2, Z$) reads as

$$\frac{\partial f_i}{\partial t} + \mathbf{v} \cdot \nabla_{\mathbf{x}} f_i = \sum_{j=A,B,C} \mathcal{Q}_i^{EL}(f_i, n_j \mathcal{M}_j) + \sum_{j=1,2,Z} \mathcal{Q}_i^{EL}(f_i, f_j) + \mathcal{Q}_i^{IN}(\mathbf{f}) + \mathcal{Q}_i^{CH}(\mathbf{f}), \quad (2.8)$$

where \mathbf{f} is the vector collecting all the distribution functions. The first sum models the elastic interactions with the host medium, the second one accounts for elastic interactions between components of the mixture. \mathcal{Q}_i^{IN} and \mathcal{Q}_i^{CH} describe the contributions of inelastic transitions and chemical reactions, respectively.

We refer to [8, 27] for a detailed description of the Boltzmann-type operators; here, we recall only that the Maxwell molecule intermolecular potential is adopted, leading to constant collision frequencies.

2.1 Linear diffusion

Starting from the kinetic description, it is possible to derive suitable reaction-diffusion systems for the number densities, performing a proper hydrodynamic limit. To this aim, we introduce a scaling in terms of a small parameter ε (standing for the Knudsen number), assuming a multi-scale interaction process.

This approach can be used to derive a reaction-diffusion system similar to the Brusselator one; in particular, we assume that

- the dominant phenomenon is constituted by elastic collisions with the host medium. Collisions of the two components of Y with the background are assumed of order $1/\varepsilon$; interactions involving the gas Z are supposed to be faster of order $1/\varepsilon^2$;
- the other elastic collisions provide a phenomenon of order ε^p ($p \geq 0$);
- inelastic interactions and the chemical reaction (2.6) are the slow process of order ε ; reaction (2.7) is assumed to be faster of order 1.

In addition, since we focus on the effects of inelastic and chemical encounters, that are of order ε , we re-scale the time by a factor ε , that, consequently, appears in front of the temporal derivatives.

We use the same procedure proposed in previous papers and we consider a proper expansion of the distribution functions (now indicated by f_i^ε , $i = 1, 2, Z$ to highlight the dependence on the small parameter ε). We observe that the evolution is dominated by collisions with the background; then

$$\sum_{j=A,B,C} \mathcal{Q}_i^{EL}(f_i^\varepsilon, n_j^\varepsilon \mathcal{M}_j) = O(\varepsilon), \quad i = 1, 2, \quad \sum_{j=A,B,C} \mathcal{Q}_i^{EL}(f_i^\varepsilon, n_j^\varepsilon \mathcal{M}_j) = O(\varepsilon^2), \quad i = Z, \quad (2.9)$$

and hence

$$f_i^\varepsilon(t, \mathbf{x}, \mathbf{v}) = n_i^\varepsilon(t, \mathbf{x}) \mathcal{M}_i(\mathbf{v}) + \varepsilon h_i^\varepsilon(t, \mathbf{x}, \mathbf{v}), \quad i = 1, 2 \quad (2.10)$$

$$f_i^\varepsilon(t, \mathbf{x}, \mathbf{v}) = n_i^\varepsilon(t, \mathbf{x}) \mathcal{M}_i(\mathbf{v}) + \varepsilon^2 h_i^\varepsilon(t, \mathbf{x}, \mathbf{v}), \quad i = Z, \quad (2.11)$$

thus

$$\int_{\mathbb{R}^3} h_i^\varepsilon(\mathbf{v}) d\mathbf{v} = 0, \quad i = 1, 2, Z. \quad (2.12)$$

By considering the weak form of the (non-dimensional) kinetic equations, by using the previous expansions (2.10) and (2.11), and by manipulating terms of the same order, we obtain the following set of partial differential equations for number densities n_1 and n_2

$$\begin{aligned} \frac{\partial n_1}{\partial t} - D_1 \Delta_{\mathbf{x}} n_1 &= a - (b + 1)n_1 + dn_1^2 n_2 \\ \frac{\partial n_2}{\partial t} - D_2 \Delta_{\mathbf{x}} n_2 &= bn_1 - dn_1^2 n_2 \end{aligned} \quad (2.13)$$

in the formal limit when $\varepsilon \rightarrow 0$. The derivation of system (2.13) is detailed in [8].

The coefficients of system (2.13) are, indeed, functions of the microscopic parameters characterizing the mixture components. More precisely,

$$a = \frac{e^{\Delta E_{B1}^{AC}} \left(\frac{m_B m_Y}{m_A m_C} \right)^{3/2} n_A n_C}{n_B}, \quad (2.14)$$

$$b = \frac{n_A \Gamma\left(\frac{3}{2}, \Theta(\Delta E_{A1}^{A2})\right) \nu_{A1}^{A2}}{n_B \Gamma\left(\frac{3}{2}, \Theta(\Delta E_{B1}^{AC})\right) \nu_{B1}^{AC}}, \quad (2.15)$$

$$d = \frac{e^{-\Delta E_{11}^{ZB}} \Gamma\left(\frac{3}{2}, \Theta(\Delta E_{Z2}^{Z1})\right) \nu_{Z2}^{Z1}}{\left(\frac{m_Y^2}{m_B m_Z}\right)^{3/2} n_B^2 \Gamma\left(\frac{3}{2}, \Theta(\Delta E_{B1}^{AC})\right) \nu_{B1}^{AC}}, \quad (2.16)$$

and

$$D_1 = \Pi \sum_{J \in \{A, B, C\}} \frac{m_J n_J \nu_{1J}}{m_Y + m_J}, \quad D_2 = \Pi \sum_{J \in \{A, B, C\}} \frac{m_J n_J \nu_{2J}}{m_Y + m_J}, \quad \Pi = \frac{\sqrt{\pi} \nu_{B1}^{AC}}{2m_Y n_B \Gamma\left(\frac{3}{2}, \Theta(\Delta E_{B1}^{AC})\right)} \quad (2.17)$$

where

- ν_{IJ} is the collision frequency associated to an elastic collision between components I and J ;
- ν_{IJ}^{HK} is the collision frequency associated to a (inelastic or chemical) transition leading I, J into H, K ;
- $\Gamma\left(\frac{3}{2}, \Theta(\Delta E)\right)$ is the incomplete Gamma function of order 3/2, where the second argument $\Theta(\Delta E)$ is a proper threshold depending on the energy gap ΔE ;
- ΔE_{IJ}^{HK} indicates the energy gap associated to a (inelastic or chemical) transition from states I, J to H, K ;

It is important to underline that, through the derivation, an explicit expression of n_Z as quadratic function of n_1 is deduced; this algebraic relation allows to reduce the number of variables in the diffusive limit.

In the following, the stability properties will be investigated in a regular open domain; if we suppose that the distribution functions f_i^ε satisfy given initial conditions at time $t = 0$ and specular reflection conditions at the boundary, then, as proved in [5], the macroscopic densities exactly obeys equations (2.13), with proper initial data and no-flux conditions at the boundary.

The procedure briefly outlined here shows that the coefficients of the macroscopic observables are positive constants that can be explicitly expressed in terms of the underlying microscopic parameters, such as collision frequencies, particle masses, and discrete energy levels. In this way, the collective behavior encoded in the macroscopic equations remains directly related to the interaction mechanisms governing the particles dynamics at the microscopic scale. This correspondence not only enhances the physical meaning of the macroscopic coefficients but also introduces natural constraints on their admissible values,

thereby delimiting the range of validity of the resulting continuum model.

As last comment, we notice that the system (2.13) is of Brusselator-type; the unique difference consists in the occurrence of coefficient d , usually equal to 1 in literature [22, 23]. The role of this parameter, and its effects on the pattern formation, will be investigated in the next section.

2.2 Nonlinear cross diffusion

A similar procedure has been used recently to derive a system with nonlinear cross diffusion in the diffusive limit. In this case we consider a different multiple scale process, where

- the dominant phenomenon is constituted by elastic collisions with the host medium, which are assumed of order $1/\varepsilon^2$;
- the other elastic collisions provide a phenomenon of order ε^p ($p \geq 0$);
- inelastic interactions and the chemical reactions proceed at order ε and ε^2 , respectively.

We rescale the time variable by a factor ε^2 .

The distribution functions are expanded as

$$f_i^\varepsilon(t, \mathbf{x}, \mathbf{v}) = n_i^\varepsilon(t, \mathbf{x}) \mathcal{M}_i(\mathbf{v}) + \varepsilon^2 h_i^\varepsilon(t, \mathbf{x}, \mathbf{v}), \quad i = 1, 2, Z, \quad (2.18)$$

since

$$\sum_{j=A,B,C} \mathcal{Q}_i^{EL}(f_i^\varepsilon, n_j^\varepsilon \mathcal{M}_j) = O(\varepsilon^2), \quad i = 1, 2, Z. \quad (2.19)$$

In the asymptotic limit, when $\varepsilon \rightarrow 0$, we get a reaction-diffusion system

$$\begin{aligned} \frac{\partial N}{\partial t} - \Delta_{\mathbf{x}} \left(\frac{D_1 \beta n_Z + D_2}{\beta n_Z + 1} N \right) &= a - \left(\frac{\beta n_Z}{\beta n_Z + 1} N \right) + c n_Z - d \left(\frac{\beta n_Z}{\beta n_Z + 1} N \right)^2 \\ \frac{\partial n_Z}{\partial t} - D_Z \Delta_{\mathbf{x}} n_Z &= -c n_Z + d \left(\frac{\beta n_Z}{\beta n_Z + 1} N \right)^2, \end{aligned} \quad (2.20)$$

where $N = n_1 + n_2$ is the total number density of the polyatomic component and the use of an algebraic relation relating n_1 , n_2 and n_Z has been made ; as shown in the previous subsection, equations are coupled with proper initial and boundary conditions. Once again, the parameters are positive constants, depending on microscopic parameters as provided below

$$a = \frac{e^{E_{B1}^{AC}} \left(\frac{m_B m_Y}{m_A m_C} \right)^{3/2} n_A n_C}{n_B}, \quad \beta = \frac{n_A \Gamma \left(\frac{3}{2}, \Theta(E_{A1}^{A2}) \right) \nu_{A1}^{A2}}{\Gamma \left(\frac{3}{2}, \Theta(E_{Z2}^{Z1}) \right) \nu_{Z2}^{Z1}}, \quad (2.21)$$

$$c = \frac{e^{E_{11}^{ZB}} \left(\frac{m_Y^2}{m_B m_Z} \right)^{3/2} \Gamma \left(\frac{3}{2}, \Theta(E_{11}^{ZB}) \right) \nu_{11}^{ZB}}{\Gamma \left(\frac{3}{2}, \Theta(E_{B1}^{AC}) \right) \nu_{B1}^{AC}}, \quad d = \frac{\Gamma \left(\frac{3}{2}, \Theta(E_{11}^{ZB}) \right) \nu_{11}^{ZB}}{n_B \Gamma \left(\frac{3}{2}, \Theta(E_{B1}^{AC}) \right) \nu_{B1}^{AC}}, \quad (2.22)$$

$$D_1 = \Pi \sum_{J \in \{A, B, C\}} \frac{m_J n_J \nu_{1J}}{m_Y + m_J}, \quad D_2 = \Pi \sum_{J \in \{A, B, C\}} \frac{m_J n_J \nu_{2J}}{m_Y + m_J}, \quad (2.23)$$

$$D_Z = \Pi \sum_{J \in \{A, B, C\}} \frac{m_J n_J \nu_{ZJ}}{m_Z + m_J}, \quad (2.24)$$

and Π is defined as in (2.17). Further details can be found in [27].

The model deduced from kinetic equations in gasdynamics presents the same diffusive terms as the predator-prey model proposed in [13] and differs from it in the reactive contributions.

3 Analysis of the Brusselator-type model

We start to discuss the possible emergence of periodic solutions in the description (2.13), and we focus on the role of the parameter d that does not appear in the classical Brusselator model.

First, we consider the steady states (and their stability) in the space homogeneous case. The system admits a unique equilibrium $E = (n_1^*, n_2^*) = (a, b/ad)$; its stability is investigated through the analysis of the linearized homogeneous problem

$$\frac{d\mathbf{U}}{dt} = \mathbf{J}\mathbf{U}, \quad (3.1)$$

where $\mathbf{U} = (n_1 - n_1^*, n_2 - n_2^*)^T$ and the jacobian matrix results

$$\mathbf{J} = \begin{pmatrix} b-1 & a^2 d \\ -b & -a^2 d \end{pmatrix}. \quad (3.2)$$

We notice that $\det \mathbf{J} = a^2 d > 0$, while the trace of \mathbf{J} is negative if and only if

$$b < 1 + a^2 d. \quad (3.3)$$

The possibility that the equilibrium becomes unstable in presence of diffusive terms will be explored under the constraint (3.3). We can already observe how the new parameter d affects both the steady state and its stability.

3.1 Turing instability

We consider now the system (2.13) in a bounded domain Ω ; we assume no-flux conditions at the boundary $\partial\Omega$. We have to discuss the solutions of the linearized system

$$\frac{\partial \mathbf{U}}{\partial t} = \mathbf{D}\Delta_{\mathbf{x}}\mathbf{U} + \mathbf{J}\mathbf{U}, \quad \text{in } \mathbb{R}_+ \times \Omega, \quad (3.4)$$

where the diffusion matrix results

$$\mathbf{D} = \begin{pmatrix} D_1 & 0 \\ 0 & D_2 \end{pmatrix}. \quad (3.5)$$

We look for solutions

$$\mathbf{U}(\mathbf{x}, t) = \sum_{k \in \mathbb{N}} c_k e^{\lambda_k t} \tilde{\mathbf{U}}_k(\mathbf{x}), \quad (3.6)$$

where the eigenfunction $\tilde{\mathbf{U}}_k$ is solution of

$$\begin{cases} \Delta_{\mathbf{x}} \tilde{\mathbf{U}}_k + k^2 \tilde{\mathbf{U}}_k = 0 & \text{in } \Omega \\ \hat{\mathbf{n}} \cdot \nabla_{\mathbf{x}} \tilde{\mathbf{U}}_k = 0 & \text{on } \partial\Omega, \end{cases} \quad (3.7)$$

being $\hat{\mathbf{n}}$ the outgoing unit vector at the boundary.

In order to have Turing instability [38], the destabilization of steady state due to spatial perturbations is needed; this results in the existence of at least a wavenumber k , such that the corresponding λ_k has positive real part. Each λ_k is solution of the dispersion relation

$$\lambda^2 + g(k^2)\lambda + h(k^2) = 0, \quad (3.8)$$

where

$$g(k^2) = k^2 \text{Tr} \mathbf{D} - \text{Tr} \mathbf{J} > 0 \quad (3.9)$$

because of relation (3.3), and

$$h(k^2) = \det(\mathbf{D})k^4 + qk^2 + \det(\mathbf{J}), \quad (3.10)$$

being $q = (1-b)D_2 + a^2dD_1$; thus, the existence of a negative solution is guaranteed by $h(k^2) < 0$; this implies that we have to impose that the minimum of h attained in

$$k_c^2 = -\frac{q}{2\det(\mathbf{D})} = -\frac{(1-b)D_2 + a^2dD_1}{D_1D_2} \quad (3.11)$$

must be negative, i.e.

$$h(k_c^2) = \frac{4\det(\mathbf{D})\det(\mathbf{J}) - q^2}{4\det(\mathbf{D})} = \frac{4a^2dD_1D_2 - [(1-b)D_2 + a^2dD_1]^2}{4D_1D_2} < 0, \quad (3.12)$$

providing

$$b < -2a\sqrt{\frac{dD_1}{D_2}} + \frac{a^2dD_1}{D_2} + 1 \quad \text{or} \quad b > 2a\sqrt{\frac{dD_1}{D_2}} + \frac{a^2dD_1}{D_2} + 1. \quad (3.13)$$

From (3.11), we have also to require that $k_c^2 > 0$, or equivalently $q < 0$, leading to

$$b > \frac{a^2 d D_1}{D_2} + 1, \quad (3.14)$$

which is compatible with constraint (3.3) if and only if $D_1 < D_2$; moreover $b > 1$. By summing up, the destabilization of the equilibrium occurs when

$$b_c := \left(1 + a \sqrt{\frac{d D_1}{D_2}} \right)^2 < b < 1 + a^2 d, \quad (3.15)$$

provided that

$$d > \frac{4 D_1 D_2}{a^2 (D_1 - D_2)^2}. \quad (3.16)$$

By expressing the coefficients in terms of the microscopic parameters of the mixture through (2.14)-(2.17) and, for illustrative purposes, without reference to any specific physical scenarios, assigning the following values

$$\begin{aligned} m_A &= 2, & m_B &= 3.5, & m_C &= 4, & m_Y &= 2.5, & m_Z &= 1.5, \\ \nu_{A1}^{A2} &= 0.008, & \nu_{Z2}^{Z1} &= 0.3, & \nu_{B1}^{AC} &= 0.001, & \nu_{11}^{ZB} &= 1, \\ \nu_{1A} &= \nu_{1B} = \nu_{1C} = \bar{\nu}_1 = 200, \\ \nu_{2A} &= \nu_{2B} = \nu_{2C} = \bar{\nu}_2 = 15, \\ n_A &= n_B = n_C = \bar{n} = 1.46, \\ E_A &= 4.5, & E_B &= 3.6, & E_C &= 4, & E_1 &= 3.9, \end{aligned} \quad (3.17)$$

we identify the values for energy levels E_2 and E_Z leading to condition (3.15) and (3.16) to be satisfied, as reported in Figure 1. In particular, we can distinguish four regions. In region I, condition (3.3) is not satisfied and the spatially homogeneous equilibrium is unstable. In regions II, III, and IV, instead, (3.3) holds, and either both conditions (3.15) and (3.16), only (3.16), or neither of the conditions in (3.15) and (3.16) are satisfied, respectively. Consequently, pattern formation can arise only when taking parameters in region II. It should be emphasized that, within region II, the parameter d is not restricted to the value 1, which once again highlights the broader spectrum of scenarios due to the presence of this additional parameter.

In the following section we perform a deeper analysis of the possible spatial configurations of the model.

3.2 Weakly nonlinear analysis

Now, we intend to investigate shapes of patterning, along with their stability, compatible with system (2.13); this can be achieved by performing a deeper analysis of the problem,

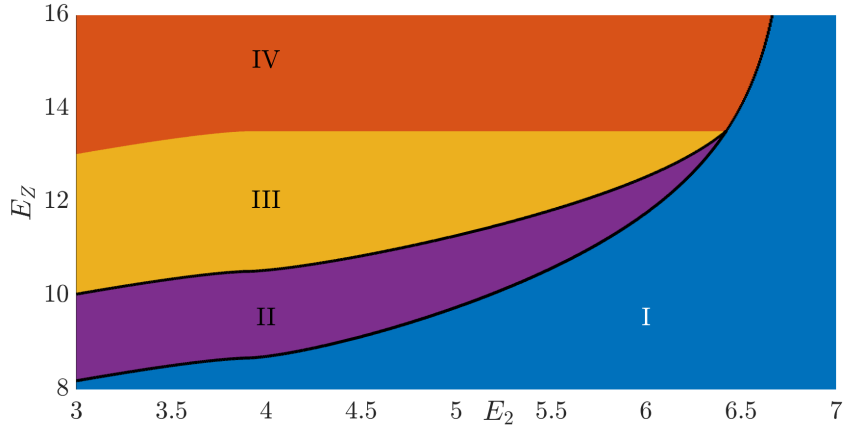


Figure 1: Values for energy levels E_2 and E_Z relevant to Turing instability for system (2.13). In region I, condition (3.3) is not satisfied, in regions II, III, and IV (3.3) holds, and either both conditions (3.15) and (3.16), only (3.16), or neither of the conditions in (3.15) and (3.16) are satisfied. Parameters are chosen as in (3.17).

performing a high order expansion of quantities involved in the model. It is worth stressing that a weakly nonlinear analysis of the classical Brusselator problem has already been discussed in literature [16, 32, 39]; therefore, here we focus on possible different patterns and/or modifications of their shape, due to specific choices of parameters in our kinetic-based model.

We consider a Taylor expansion of system (2.13) up to the third order around the equilibrium (n_1^*, n_2^*) , obtaining

$$\frac{\partial \mathbf{U}}{\partial t} = \mathcal{L} \mathbf{U} + \mathcal{H}[\mathbf{U}], \quad \text{for } \mathbf{U} = \begin{pmatrix} U \\ V \end{pmatrix} = \begin{pmatrix} n_1 - n_1^* \\ n_2 - n_2^* \end{pmatrix} \quad (3.18)$$

with

$$\mathcal{L} = \mathbf{D} \Delta_{\mathbf{x}} + \mathbf{J} \quad (3.19)$$

where \mathbf{J} and \mathbf{D} are the Jacobian and the diffusion matrix, respectively, while

$$\mathcal{H}[\mathbf{U}] = \begin{pmatrix} (-1+b)U + \frac{2b}{a}U^2 + a^2dV + 4adUV + 6dU^2V \\ -bU - \frac{2b}{a}U^2 - a^2dV - 4adUV - 6dU^2V \end{pmatrix}. \quad (3.20)$$

Keeping in mind the necessary conditions (3.15) for spatial pattern formation (in terms of the parameter b), we define the critical value allowing for Turing instability. In accordance with the choice of parameters made in (3.17), we have that the diffusion coefficient $D_1 = 1$, this choice streamlines the calculations without being restrictive, since conditions (3.15)-(3.16) only depend on the ratio D_2/D_1 ; in addition, we define $\xi := \sqrt{\frac{1}{D_2}}$, obtaining

$$b_c = \left(1 + a\xi\sqrt{d}\right)^2 \quad (3.21)$$

and the critical wavenumber

$$k_c^2 = a\xi\sqrt{d}, \quad (3.22)$$

such that $\det(\mathbf{J} - k_c^2 \mathbf{D}) = 0$ and $\det(\mathbf{J} - k \mathbf{D}) > 0$ for some wavenumber k , when $b > b_c$.

At this stage, we take advantage of the fact that the system's dynamics evolve more slowly, when the parameter b is close to the critical threshold. This slower evolution allows us to study pattern formation using amplitude equations. Therefore, to better understand this scenario, we express the bifurcation parameter b as follows

$$b = b_c + \eta b_1 + \eta^2 b_2 + \eta^3 b_3 + O(\eta^3), \quad (3.23)$$

where η is a small parameter; we expand also the solution vector \mathbf{U} in terms of η

$$\mathbf{U} = \eta \begin{pmatrix} U_1 \\ V_1 \end{pmatrix} + \eta^2 \begin{pmatrix} U_2 \\ V_2 \end{pmatrix} + \eta^3 \begin{pmatrix} U_3 \\ V_3 \end{pmatrix} + O(\eta^3). \quad (3.24)$$

As already pointed out, when the bifurcation parameter is near its critical threshold, the amplitude of the emerging pattern evolves slowly over time. This separation of time scales enables us to distinguish between fast and slow temporal dynamics. As a result, we can introduce a multiple time scale framework, such that

$$\frac{\partial}{\partial t} = \eta \frac{\partial}{\partial T_1} + \eta^2 \frac{\partial}{\partial T_2} + O(\eta^2). \quad (3.25)$$

By substituting the expansions (3.24)–(3.25) into system (3.18) and collecting terms of the same order in η , we obtain the following set of equations at successive orders:

- order η :

$$\mathcal{L}_c \left[\begin{pmatrix} U_1 \\ V_1 \end{pmatrix} \right] = 0 \quad (3.26)$$

with

$$\mathcal{L}_c = \begin{bmatrix} b_c - 1 + \Delta_x & a^2 d \\ -b_c & -a^2 d + \frac{1}{\xi^2} \Delta_x \end{bmatrix}, \quad (3.27)$$

- order η^2 :

$$\frac{\partial}{\partial T_1} \left(\begin{pmatrix} U_1 \\ V_1 \end{pmatrix} \right) = \mathcal{L}_c \left[\begin{pmatrix} U_2 \\ V_2 \end{pmatrix} \right] + \mathcal{H}_2 \left[\begin{pmatrix} U_1 \\ V_1 \end{pmatrix} \right] \quad (3.28)$$

with

$$\mathcal{H}_2 \left[\begin{pmatrix} U_1 \\ V_1 \end{pmatrix} \right] = \begin{bmatrix} b_1 U_1 + \frac{b_c U_1^2}{a} + 2adU_1V_1 + a^2dV_2 \\ -b_1 U_1 - \frac{b_c U_1^2}{a} - 2adU_1V_1 \end{bmatrix} \quad (3.29)$$

- order η^3 :

$$\frac{\partial}{\partial T_1} \begin{pmatrix} U_2 \\ V_2 \end{pmatrix} + \frac{\partial}{\partial T_2} \begin{pmatrix} U_1 \\ V_1 \end{pmatrix} = \mathcal{L}_c \left[\begin{pmatrix} U_3 \\ V_3 \end{pmatrix} \right] + \mathcal{H}_3 \left[\begin{pmatrix} U_1 \\ V_1 \end{pmatrix}, \begin{pmatrix} U_2 \\ V_2 \end{pmatrix} \right] \quad (3.30)$$

$$\mathcal{H}_3 \left[\begin{pmatrix} U_1 \\ V_1 \end{pmatrix}, \begin{pmatrix} U_2 \\ V_2 \end{pmatrix} \right] = \begin{bmatrix} b_2 U_1 + \frac{b_1 U_1^2}{a} + b_1 U_2 + \frac{2b_c U_1 U_2}{a} \\ + d U_1^2 V_1 + 2ad U_2 V_1 + 2ad U_1 V_2 \\ - b_2 U_1 - \frac{b_1 U_1^2}{a} - b_1 U_2 - \frac{2b_c U_1 U_2}{a} \\ - d U_1^2 V_1 - 2ad U_2 V_1 - 2ad U_1 V_2 \end{bmatrix}. \quad (3.31)$$

By solving system (3.26), and leveraging the spectral properties of the operator \mathcal{L}_c , the solution can be expressed in terms of three dominant active pairs of eigenmodes $(\mathbf{k}_j, -\mathbf{k}_j)$, for $j = 1, 2, 3$. These modes correspond to wavevectors with equal magnitude $|\mathbf{k}_j| = k_c$ and are oriented at angles separated by $2\pi/3$, satisfying the condition $\mathbf{k}_1 + \mathbf{k}_2 + \mathbf{k}_3 = \mathbf{0}$ [31]. The solution thus takes the form:

$$\begin{pmatrix} U_1 \\ V_1 \end{pmatrix} = \begin{pmatrix} \rho \\ 1 \end{pmatrix} \sum_{j=1}^3 [\mathcal{W}_j(t) e^{i \mathbf{k}_j \cdot \mathbf{x}} + \overline{\mathcal{W}}_j(t) e^{-i \mathbf{k}_j \cdot \mathbf{x}}], \quad (3.32)$$

where $\overline{\mathcal{W}}_j$ is the complex conjugate of \mathcal{W}_j , and $\rho = -\frac{a\sqrt{d}}{\xi + a\xi^2\sqrt{d}}$.

Now, we move to discuss terms of order η^2 (3.28), that can be recast as

$$\mathcal{L}_c \left[\begin{pmatrix} U_2 \\ V_2 \end{pmatrix} \right] = \frac{\partial}{\partial T_1} \begin{pmatrix} U_1 \\ V_1 \end{pmatrix} - \mathcal{H}_2 \left[\begin{pmatrix} U_1 \\ V_1 \end{pmatrix} \right]; \quad (3.33)$$

the existence of a nontrivial solution $(U_2, V_2)^T$ to this non-homogeneous system (3.33) is guaranteed by the Fredholm solvability condition. According to it, the right-hand side of equation (3.33) must be orthogonal to the kernel of the adjoint operator \mathcal{L}_c^+ of \mathcal{L}_c , whose corresponding eigenvectors are given by

$$\begin{pmatrix} 1 \\ \sigma \end{pmatrix} e^{i \mathbf{k}_j \cdot \mathbf{x}} + \text{c.c.}, \quad (3.34)$$

where by c.c. we indicate the complex conjugate of the first term in (3.34) and $\sigma = \frac{a\xi\sqrt{d}}{1 + a\xi\sqrt{d}}$.

The right-hand side of (3.33) can be expressed as a linear combination of the terms e^0 , $e^{i \mathbf{k}_j \cdot \mathbf{x}}$, $e^{2i \mathbf{k}_j \cdot \mathbf{x}}$, and $e^{i(\mathbf{k}_j - \mathbf{k}_l) \cdot \mathbf{x}}$. Isolating the coefficients associated with the terms $e^{i \mathbf{k}_j \cdot \mathbf{x}}$, we get

$$\begin{pmatrix} R_U^j \\ R_V^j \end{pmatrix} = \begin{pmatrix} \rho \\ 1 \end{pmatrix} \frac{\partial \mathcal{W}_j}{\partial T_1} + \begin{pmatrix} -1 \\ 1 \end{pmatrix} \left[\rho b_1 W_j + 4\rho \left(ad + \frac{2\rho b_c}{a} \right) \overline{\mathcal{W}}_l \overline{\mathcal{W}}_m \right], \quad (3.35)$$

with $l, m \neq j$, and $l \neq m$.

It follows that the solvability condition provides

$$(\rho + \sigma) \frac{\partial \mathcal{W}_j}{\partial T_1} = (1 - \sigma) \left[\rho b_1 W_j + 4\rho \left(ad + \frac{2\rho b_c}{a} \right) \bar{\mathcal{W}}_l \bar{\mathcal{W}}_m \right], \quad (3.36)$$

for $j = 1, 2, 3$.

At this point, it is reasonable to expect the solution of (3.33) to be of the form

$$\begin{aligned} \begin{pmatrix} U_2 \\ V_2 \end{pmatrix} = & \begin{pmatrix} X_0 \\ Y_0 \end{pmatrix} (|\mathcal{W}_1|^2 + |\mathcal{W}_2|^2 + |\mathcal{W}_3|^2) \\ & + \sum_{j=1}^3 \begin{pmatrix} \rho \\ 1 \end{pmatrix} \mathcal{V}_j e^{i \mathbf{k}_j \cdot \mathbf{x}} + \sum_{j=1}^3 \begin{pmatrix} X_2 \\ Y_2 \end{pmatrix} \mathcal{W}_j^2 e^{2i \mathbf{k}_j \cdot \mathbf{x}} \\ & + \sum_{\substack{j=1,2,3 \\ l \equiv j+1 \pmod{3}}} \begin{pmatrix} X_1 \\ Y_1 \end{pmatrix} \mathcal{W}_j \bar{\mathcal{W}}_l e^{i(\mathbf{k}_j - \mathbf{k}_l) \cdot \mathbf{x}} + \text{c.c.}, \end{aligned} \quad (3.37)$$

where here c.c. collect the complex conjugates of the explicit terms on the right-hand side.

By manipulating (3.33), the coefficients X_m, Y_m can be obtained from the linear equations for $e^0, e^{i \mathbf{k}_j \cdot \mathbf{x}}, e^{2i \mathbf{k}_j \cdot \mathbf{x}}, e^{i(\mathbf{k}_j - \mathbf{k}_l) \cdot \mathbf{x}}$

$$\begin{aligned} \begin{pmatrix} X_0 \\ Y_0 \end{pmatrix} &= \begin{pmatrix} 0 \\ -\frac{2\rho}{a} \left(2 + \frac{\rho b_c}{a^2 d} \right) \end{pmatrix} \\ \begin{pmatrix} X_2 \\ Y_2 \end{pmatrix} &= \frac{\rho (2a^2 d + b_c \rho)}{4a k_c^2 (1 - b_c + 4k_c^2) + a^3 d (1 + 4k_c^2) \xi^2} \begin{pmatrix} 4k_c^2 \\ -(1 + 4k_c^2) \xi^2 \end{pmatrix} \\ \begin{pmatrix} X_1 \\ Y_1 \end{pmatrix} &= \frac{2\rho (2a^2 d + b_c \rho)}{3a k_c^2 (1 - b_c + 3k_c^2) + a^3 d (1 + 3k_c^2) \xi^2} \begin{pmatrix} 3k_c^2 \\ -(1 + 3k_c^2) \xi^2 \end{pmatrix}. \end{aligned} \quad (3.38)$$

Lastly, we proceed to the equation at order η^3 , given in (3.30), which can be rewritten as follows

$$\mathcal{L}_c \left[\begin{pmatrix} U_3 \\ V_3 \end{pmatrix} \right] = \frac{\partial}{\partial T_1} \begin{pmatrix} U_2 \\ V_2 \end{pmatrix} + \frac{\partial}{\partial T_2} \begin{pmatrix} U_1 \\ V_1 \end{pmatrix} - \mathcal{H}_3 \left[\begin{pmatrix} U_1 \\ V_1 \end{pmatrix}, \begin{pmatrix} U_2 \\ V_2 \end{pmatrix} \right]. \quad (3.39)$$

Substituting expressions (3.32) and (3.37) into (3.39), together with the relations in (3.36), we can apply the Fredholm solvability condition, which yields

$$\begin{aligned} (\rho + \sigma) \left(\frac{\partial \mathcal{V}_j}{\partial T_1} + \frac{\partial \mathcal{W}_j}{\partial T_2} \right) = & (1 - \sigma) \left[b_2 \rho W_j + b_1 \rho \left(\mathcal{V}_j + \frac{2\rho}{a} \bar{\mathcal{W}}_m \bar{\mathcal{W}}_l \right) \right. \\ & \left. + r_1 (\bar{\mathcal{V}}_l \bar{\mathcal{W}}_m + \bar{\mathcal{V}}_m \bar{\mathcal{W}}_l) + r_2 |\mathcal{W}_j|^2 + r_3 (|\mathcal{W}_l|^2 + |\mathcal{W}_m|^2) \mathcal{W}_j \right], \end{aligned} \quad (3.40)$$

for $j, l, m = 1, 2, 3$, $j \neq l \neq m$, where the coefficients are

$$\begin{aligned} r_1 &= \frac{2\rho(2a^2 + b_c\rho)}{a}, \\ r_2 &= \frac{2b_cX_2\rho}{a} + 3\rho^2 + 2a(X_2 + (Y_0 + Y_2)\rho), \\ r_3 &= 2aX_1 + \frac{2(b_cX_1 + a^2Y_0 + a^2Y_1)\rho}{a} + 6\rho^2. \end{aligned} \quad (3.41)$$

Upon combining equations (3.32) and (3.37), the amplitude is recovered in its explicit expanded form

$$\mathbf{A}_j = \eta \begin{pmatrix} \rho \\ 1 \end{pmatrix} \mathcal{W}_j + \eta^2 \begin{pmatrix} \rho \\ 1 \end{pmatrix} \mathcal{V}_j + O(\eta^3), \quad j = 1, 2, 3, \quad (3.42)$$

where $\mathbf{A}_j = (A_j^U, A_j^V, A_j^W)^T$ denotes the amplitude vector associated with the mode \mathbf{k}_j . Then we arrive at the governing equations for the amplitudes, given by

$$\frac{\partial \mathbf{A}_j}{\partial t} = \eta^2 \begin{pmatrix} \rho \\ 1 \end{pmatrix} \frac{\partial \mathcal{W}_j}{\partial T_1} + \eta^3 \begin{pmatrix} \rho \\ 1 \end{pmatrix} \left(\frac{\partial \mathcal{W}_j}{\partial T_2} + \frac{\partial \mathcal{V}_j}{\partial T_1} \right) + O(\eta^4), \quad j = 1, 2, 3. \quad (3.43)$$

Accordingly, from equations (3.36)–(3.40), we obtain the evolution equation governing A_j^U :

$$r_0 \frac{\partial A_j^U}{\partial t} = \mu A_j^U + (s_1 + \mu \tilde{s}_1) \overline{A_l^U} \overline{A_m^U} + A_j^U [s_2 |A_j^U|^2 + s_3 (|A_l^U|^2 + |A_m^U|^2)], \quad (3.44)$$

being

$$r_0 = \frac{\rho + \sigma}{b_c \rho (1 - \sigma)}, \quad \mu = \frac{b - b_c}{b_c}, \quad s_1 = \frac{4ad}{b_c \rho} + \frac{2}{a}, \quad \tilde{s}_1 = \frac{2}{a}, \quad s_i = \frac{r_0 r_i}{\rho^3}, \quad i = 2, 3; \quad (3.45)$$

an analogous expression holds for A_j^V .

We represent each amplitude in terms of its modulus and phase angle, writing $A_j^U = \rho_j e^{i\phi_j}$. By substituting these expressions into system (3.44) and equating the real and imaginary components separately, we derive the following set of equations

$$\begin{aligned} r_0 \frac{\partial \phi}{\partial t} &= -(s_1 + \mu \tilde{s}_1) \frac{\rho_1^2 \rho_2^2 + \rho_2^2 \rho_3^2 + \rho_1^2 \rho_3^2}{\rho_1 \rho_2 \rho_3} \sin(\phi) \\ r_0 \frac{\partial \rho_1}{\partial t} &= \mu \rho_1 + (s_1 + \mu \tilde{s}_1) \rho_2 \rho_3 \cos(\phi) + s_2 \rho_1^3 + s_3 (\rho_2^2 + \rho_3^2) \rho_1 \\ r_0 \frac{\partial \rho_2}{\partial t} &= \mu \rho_2 + (s_1 + \mu \tilde{s}_1) \rho_1 \rho_3 \cos(\phi) + s_2 \rho_2^3 + s_3 (\rho_1^2 + \rho_3^2) \rho_2 \\ r_0 \frac{\partial \rho_3}{\partial t} &= \mu \rho_3 + (s_1 + \mu \tilde{s}_1) \rho_1 \rho_2 \cos(\phi) + s_2 \rho_3^3 + s_3 (\rho_1^2 + \rho_2^2) \rho_3, \end{aligned} \quad (3.46)$$

being $\phi = \phi_1 + \phi_2 + \phi_3$.

The stationary solutions of system (3.46) correspond to the distinct observable patterns. In particular, we can identify the following cases:

Table 1: Classification of steady states of system (3.46) (stripes \mathcal{S} , hexagons $\mathcal{H}_l^\pm, l = 0, \pi$) in each region of Figure 2.

Region	Stable Equilibria
I	$\mathcal{S}, \mathcal{H}_0^-$
II	\mathcal{H}_0^-
III	\mathcal{S}
IV	$\mathcal{S}, \mathcal{H}_\pi^-$
V	\mathcal{H}_π^-

i) Homogeneous solution with $\rho_1 = \rho_2 = \rho_3 = 0$; in this case, no pattern emerges.

ii) Striped pattern $\mathcal{S} = (\phi, \rho_1, 0, 0)$, with $\rho_1 = \sqrt{-\frac{\mu}{s_2}}$;

iii) Hexagonal patterns, $\mathcal{H}_\phi^\pm = (\bar{\phi}, \bar{\rho}_\pm, \bar{\rho}_\pm, \bar{\rho}_\pm)$, with

$$\bar{\phi} = \frac{\pi}{2} (1 + \text{sign}(s_1 + \mu \tilde{s}_1)),$$

$$\bar{\rho}_\pm = \frac{|s_1 + \mu \tilde{s}_1| \pm \sqrt{-4(s_2 + 2s_3)\mu + (s_1 + \mu \tilde{s}_1)^2}}{2(s_2 + 2s_3)};$$

iv) Mixed patterns, $\mathcal{M}_{\tilde{\phi}} = (\tilde{\phi}, \tilde{\rho}_1, \tilde{\rho}_2, \tilde{\rho}_2)$, with

$$\tilde{\phi} = \frac{\pi}{2} \left(1 - \text{sign} \left(\frac{s_1 + \mu \tilde{s}_1}{s_2 - s_3} \right) \right),$$

$$\tilde{\rho}_1 = \left| \frac{s_1 + \mu \tilde{s}_1}{s_2 - s_3} \right|, \quad \tilde{\rho}_2 = \sqrt{\frac{-\mu - s_2 \rho_1^2}{s_2 + s_3}}.$$

We observe that, although the types of patterns identified for a generic value of parameter d (in the range of interest) are the same as those obtained in the case $d = 1$ [32, 39], the new parameter still plays a role by influencing the pattern amplitude.

To best highlight the variety of scenarios, discuss the existence and stability of the emerging patterns, and thus confirm and extend the results available in the literature [32, 39], we choose to fix the parameters as in (3.17) and let the internal energies vary. We can observe that, within the range of parameters providing Turing instability (region II of Figure 1), five regions of interest can be identified, as shown in Figure 2); in each region at least one of the patterns individuated above is stable, as reported in Table 1. The thick black lines delimit region II of Figure 1, while the blue area corresponds to region I in Figure 1, where the equilibrium is unstable and Turing instability cannot occur.

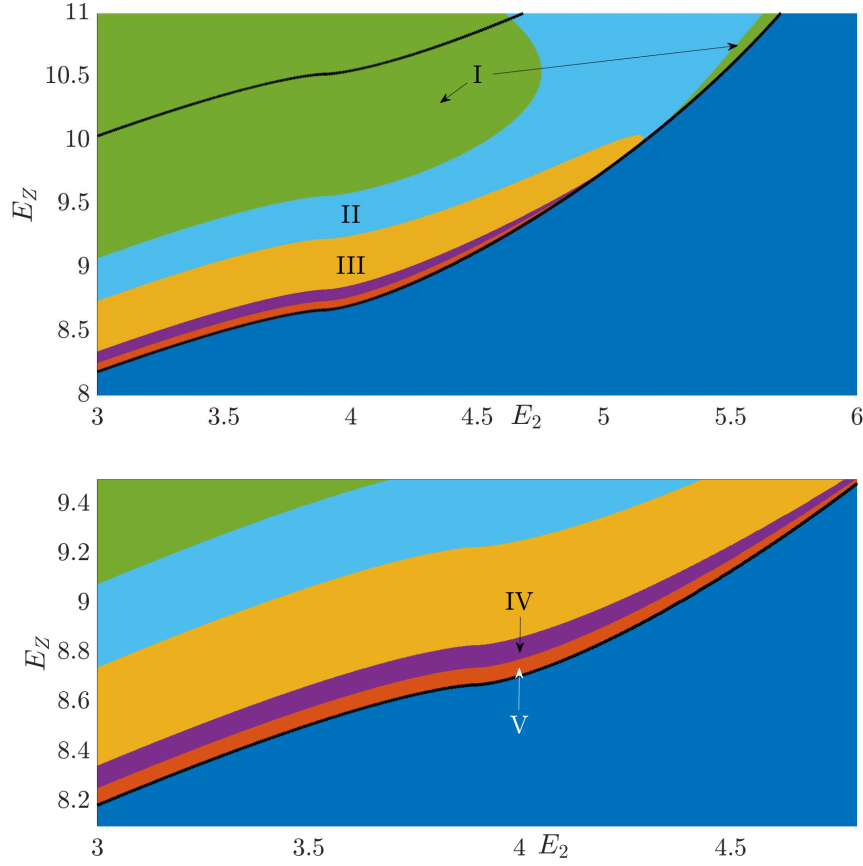


Figure 2: Values for energy levels E_2 and E_Z relevant to the stability of the different patterns system (2.13), as reported in Table 1. Black lines define the region where Turing instability can occur. Parameters are chosen as in (3.17).

3.3 Numerical simulations

In this section we investigate the behavior of system (2.13) by performing numerical simulations. We simulate a two-dimensional square domain of length $L = 12\pi$, discretized into a 100×100 grid. The solution is initialized by adding a random perturbation to the equilibrium values. The diffusive terms are discretized using a second-order finite-difference method, the source terms are evaluated locally, and the solution is marched in time from the initial conditions until convergence using a first-order forward-Euler scheme. It is worth noting that once the solution is converged to a steady state, the error associated with the time discretization vanishes. Therefore, using a first-order time-integration scheme is acceptable for our purposes. The time step is dynamically adapted throughout the simulation to maintain numerical stability by keeping the local von Neumann number - determined from the maximum diffusion coefficient in the domain - under a given threshold. At the boundary of the domain, we impose zero-gradient Neumann conditions. We do so by utilizing a layer of ghost cells and adapting their value as the simulation evolves.

Table 2: Values of coefficients for macroscopic system (2.13) taking microscopic values as in (3.17), for different choices of E_2 and E_Z .

Case	E_2	E_Z	a	b	d	D_1	D_2	Region
1	3.81	8.68	4.53	8	2.11	1	13.33	V
2	3.78	8.76	4.53	8	1.93	1	13.33	IV
3	3.65	8.90	4.53	8	1.59	1	13.33	III

The method is implemented in a modified version of the open-source Hyper2D solver [9] tailored to reaction-diffusion systems.

At this point, we confirm the results obtained in the previous subsection by letting E_2 and E_Z vary in the region of parameters where spatially non-homogeneous configurations are expected. We fix again parameters as in (3.17) and we select three cases corresponding to different values of E_2 and E_Z ; the chosen cases provide an exhaustive overview of emerging patterns. The relevant coefficients of the macroscopic system (2.13) in each case are reported in Table 2.

Case 1. We start by taking values of E_2 and E_Z in region V, more precisely $E_2 = 3.81$ and $E_Z = 8.68$ (row 1 in Table 2). We run this simulation and the following ones up to final time $t = 1000$. Accordingly to the analysis, we observe the formation of hexagonal pattern corresponding to phase $\phi = \pi$, as shown in Figure 3.

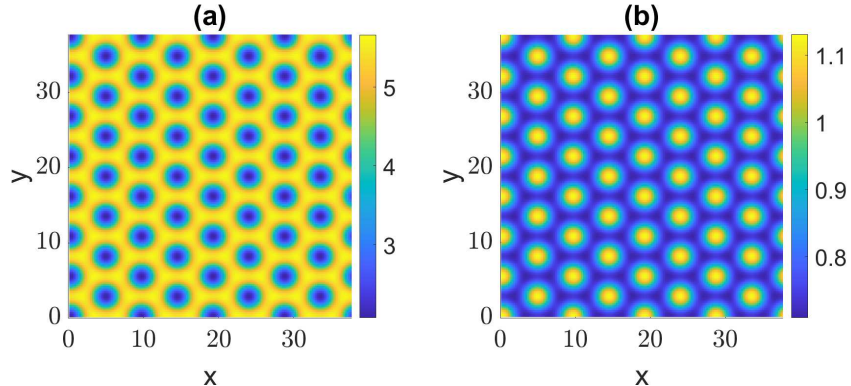


Figure 3: Pattern formation for system (2.13) in a squared domain Ω assuming no-flux conditions at the boundary $\partial\Omega$, and taking coefficient as reported in the first row of Table 2. Panel (a): density of n_1 . Panel (b): density of n_2 .

Case 2. We take values of E_2 and E_Z in region IV, more precisely $E_2 = 3.78$ and $E_Z = 8.76$ (row 2 in Table 2). In accordance with the analysis in the previous subsection, we observe the coexistence of hexagonal and striped patterns, as shown in Figure 4.

Case 3. We consider E_2 and E_Z in region III, more precisely $E_2 = 3.65$ and $E_Z = 8.90$ (row 3 in Table 2). As predicted by weakly nonlinear analysis, we observe the formation of striped pattern, as shown in Figure 5.

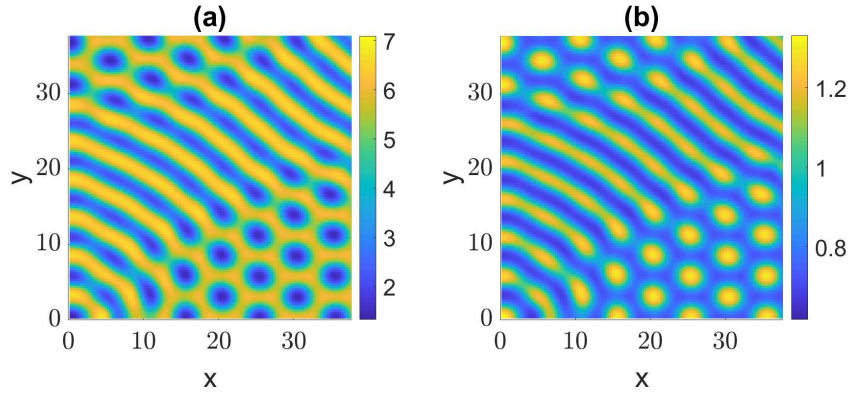


Figure 4: Pattern formation for system (2.13) in a squared domain Ω assuming no-flux conditions at the boundary $\partial\Omega$, and taking coefficient as reported in the second row of Table 2. Panel (a): density of n_1 . Panel (b): density of n_2 .

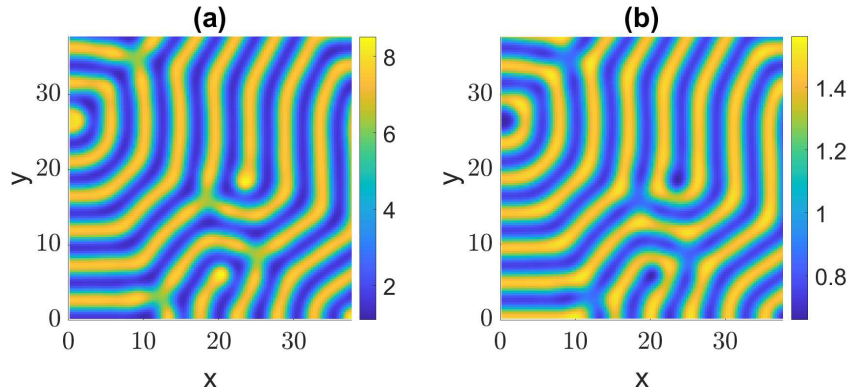


Figure 5: Pattern formation for system (2.13) in a squared domain Ω assuming no-flux conditions at the boundary $\partial\Omega$, and taking coefficient as reported in the third row of Table 2. Panel (a): density of n_1 . Panel (b): density of n_2 .

For the sake of brevity, we do not report the patterns in regions I and II, since their shape is similar to that of the patterns in regions IV and V, respectively; the only difference concerns the phase angle ϕ , which passes from π to 0, giving rise to the so-called reentrant hexagons [39]. Although our model includes an additional parameter d , it reproduces qualitatively the same types of patterns reported in the literature [32], albeit with some quantitative differences. Different parameter values, as well as different choices of the initial datum, lead to different patterns; the different ways in which instabilities interact with nonlinearities can sometimes result in the coexistence of multiple pattern types, as illustrated in Figure 4.

4 Pattern formation in the model with nonlinear cross diffusion

We move now to system (2.20), with the scope to investigate the two-dimensional formation of patterns, extending the results outlined in [27] in the one-dimensional setting. Proceeding as in the previous case, we start by observing that the space homogeneous version of system (2.20) has a unique steady state

$$E = (N^*, n_Z^*) = \left(a + \frac{ac}{\zeta}, \frac{\xi}{c} \right), \quad (4.1)$$

with $\zeta = a^2 d \beta$ and $\xi = a^2 d$, whose stability can be analyzed by investigating the linearized problem for $\mathbf{U} = (N - N^*, n_Z - n_Z^*)^T$

$$\frac{d\mathbf{U}}{dt} = \mathbf{J}\mathbf{U}, \quad (4.2)$$

where the jacobian matrix evaluated at the equilibrium is

$$\mathbf{J} = \begin{pmatrix} -\frac{\zeta\nu}{c+\zeta} & c - a\frac{c^2\nu}{\xi(c+\zeta)} \\ \frac{\zeta(-1+\nu)}{c+\zeta} & c\frac{c-\zeta}{c+\zeta} \end{pmatrix}, \quad (4.3)$$

with $\nu = 1 + 2ad$. We observe that

$$\text{tr}(\mathbf{J}) = \frac{c^2 - \zeta(c + \nu)}{c + \zeta} \text{ and } \det(\mathbf{J}) = \frac{c\zeta}{c + \zeta} > 0, \quad (4.4)$$

and hence we have to require

$$\text{tr}(\mathbf{J}) < 0 \iff \beta > \frac{c^2}{\xi(c + \nu)} =: \bar{\beta} \quad (4.5)$$

to guarantee the stability of the equilibria.

4.1 Turing instability and weakly nonlinear analysis

In presence of diffusion, the linearized problem results

$$\frac{\partial \mathbf{U}}{\partial t} = \mathbf{D}\Delta_{\mathbf{x}}\mathbf{U} + \mathbf{J}\mathbf{U}, \quad (4.6)$$

where the diffusion matrix is given by

$$\mathbf{D} = \begin{pmatrix} \frac{\zeta D_1 + c D_2}{c + \zeta} & \frac{c^2(D_1 - D_2)}{ad(c + \zeta)} \\ 0 & D_Z \end{pmatrix}. \quad (4.7)$$

As in the previous case, we look for solutions of the form given in (3.6)-(3.7), and the Turing instability is related to the existence of at least a wavenumber k , such that the corresponding λ_k has positive real part. Each λ_k is solution of the usual dispersion relation

$$\lambda^2 + g(k^2)\lambda + h(k^2) = 0, \quad (4.8)$$

where

$$g(k^2) = k^2 \text{Tr} \mathbf{D} - \text{Tr} \mathbf{J} > 0 \quad (4.9)$$

because of relation (4.5), and

$$h(k^2) = \det(\mathbf{D})k^4 + qk^2 + \det(\mathbf{J}), \quad (4.10)$$

$$\text{being } q = \frac{c(\zeta D_1 - cD_2) + \nu \zeta D_Z}{c + \zeta}.$$

We have to require that the minimum of h attained in

$$k_c^2 = -\frac{q}{2 \det(\mathbf{D})} = -\frac{c(\zeta D_1 - cD_2) + \nu \zeta D_Z}{2(\zeta D_1 + cD_2)D_Z} \quad (4.11)$$

must be negative, i.e.

$$h(k_c^2) = \frac{4 \det(\mathbf{D}) \det(\mathbf{J}) - q^2}{4 \det(\mathbf{D})} = \frac{4c\xi D_Z(\zeta D_1 + cD_2)\beta - [c(\zeta D_1 - cD_2) + \nu \zeta D_Z]^2}{4D_Z(c + \zeta)(\zeta D_1 + cD_2)} < 0, \quad (4.12)$$

or, equivalently,

$$p(D_2) = c^4 D_2^2 - 2D_2 c^2 \zeta (cD_1 + D_Z(2 + \nu)) + \zeta^2 ((cD_1 + \nu D_Z)^2 - 4cD_1 D_Z) > 0. \quad (4.13)$$

The positivity of k_c^2 in (4.11) provides the constraint

$$D_2 > \frac{\zeta (cD_1 + D_Z \nu)}{c^2} =: \hat{D}_2. \quad (4.14)$$

We can now observe that $p(D_2) > 0$ if and only if $D_2 < D_2^- \vee D_2 > D_2^+$, where

$$D_2^\pm = \frac{\zeta}{c^2} \left(cD_1 + D_Z(2 + \nu) \pm 2\sqrt{D_Z(2cD_1 + D_Z(1 + \nu))} \right)$$

are both positive values. Moreover, it holds

$$p(\hat{D}_2) = -4D_Z \zeta^2 (2cD_1 + D_Z \nu), \quad (4.15)$$

which is negative; hence, by continuity arguments, the necessary conditions for the Turing instability are fulfilled in a right neighborhood of D_2^+ , and we define the critical threshold $D_2^c := D_2^+$, obtaining the constraint

$$D_2 > D_2^c = \frac{\zeta}{c^2} \left(cD_1 + D_Z(2 + \nu) + 2\sqrt{D_Z(2cD_1 + D_Z(1 + \nu))} \right). \quad (4.16)$$

As in the previous case, we want to focus on the microscopic features of the model, by finding suitable sets of the microscopic parameters that lead to the conditions above to be satisfied by the macroscopic coefficients, through the relations (2.21)-(2.23). For our purposes, we assign the following values as an illustrative example, without referring to any specific physical scenarios

$$\begin{aligned}
m_A &= 3, & m_B &= 5.31, & m_C &= 5, & m_Y &= 2.69, & m_Z &= 0.07, \\
\nu_{A1}^{A2} &= 0.2, & \nu_{Z2}^{Z1} &= 0.4, & \nu_{B1}^{AC} &= 0.0001, & \nu_{11}^{ZB} &= 0.002, \\
\nu_{1A} &= \nu_{1B} = \nu_{1C} = 80, \\
\nu_{ZA} &= \nu_{ZB} = \nu_{ZC} = 994.5, \\
n_A &= 32.8, & n_B &= 2.38, & n_C &= 1, \\
E_A &= 0.5, & E_B &= 0.5, & E_C &= 0.5, & E_1 &= 3, & E_Z &= 1.5; \\
\end{aligned} \tag{4.17}$$

consequently, we reduce to discuss the parameter range of interest in terms of the energy level E_2 and of the collision frequencies of the polyatomic component with the background $\nu_{2A} = \nu_{2B} = \nu_{2C} =: \bar{\nu}_2$, in such a way that the macroscopic coefficients satisfy conditions (4.5)-(4.16). In Figure 6, we individuate three regions in the $E_2 - \bar{\nu}_2$ plane: in region III, condition (4.5) does not hold, thus the spatially homogeneous equilibrium is unstable and patterns cannot form; in region I only (4.5) is fulfilled, while in II both (4.5) and (4.16) are satisfied. Therefore, the emergence of spatial patterns must be investigated in region II.

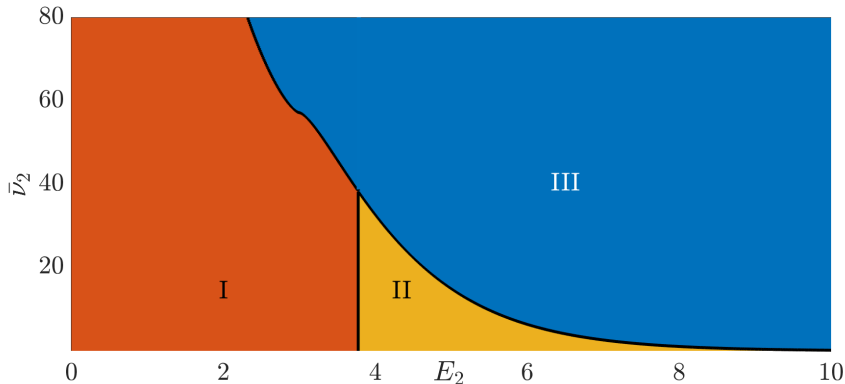


Figure 6: Values for energy level E_2 and collision frequency $\bar{\nu}_2$ relevant to Turing instability for system (2.20). In region III, condition (4.5) is not satisfied, in region I only (4.5) is fulfilled, while in II both (4.5) and (4.16) hold. Parameters are chosen as in (4.17).

As done before, a weakly nonlinear analysis of the problem is performed; then, a third order Taylor expansion around the equilibrium system (N^*, n_Z^*) leads to

$$\frac{\partial \mathbf{U}}{\partial t} = \mathcal{L} \mathbf{U} + \mathcal{H}[\mathbf{U}], \quad \text{for} \quad \mathbf{U} = \begin{pmatrix} U \\ V \end{pmatrix} = \begin{pmatrix} N - N^* \\ n_Z - n_Z^* \end{pmatrix}, \tag{4.18}$$

with $\mathcal{L} = \mathbf{D}\Delta_{\mathbf{x}} + \mathbf{J}$, being \mathbf{J} and \mathbf{D} the Jacobian and the diffusion matrix, respectively, while the nonlinear part of the expansion $\mathcal{H}[\mathbf{U}] = (\mathcal{H}^U[\mathbf{U}], \mathcal{H}^V[\mathbf{U}])^T$ has the following components

$$\begin{aligned} \mathcal{H}^U[\mathbf{U}] = & -\frac{3\beta^2 c^4 \delta \Delta V V^2}{ad(c+\zeta)^3} + \frac{\beta c^4 V^3(-a\beta + 2c - 2\zeta)}{\xi(c+\zeta)^3} + \frac{2\beta c^3 \delta \Delta V V}{ad(c+\zeta)^2} + \frac{2\beta c^3 \delta (\nabla V)^2}{ad(c+\zeta)^2} \\ & + \frac{\beta c^3 U V^2(a\beta - 2c + 4\zeta)}{a(c+\zeta)^3} + \frac{c^3 V^2(a\beta - c + 2\zeta)}{\xi(c+\zeta)^2} - \frac{c^2 \delta \Delta V}{ad(c+\zeta)} \\ & - \frac{\zeta U(a+2\xi)}{a(c+\zeta)} - \frac{c V(a\beta c + \zeta(c-\zeta))}{\zeta(c+\zeta)} + \frac{2\beta c^3 \delta \Delta V \zeta U V}{\xi(c+\zeta)^3} + \frac{4\beta c^3 \delta \zeta V \nabla U \nabla V}{\xi(c+\zeta)^3} \\ & + \frac{\beta^2 c^3 \delta \Delta U V^2}{(c+\zeta)^3} - \frac{2\beta c^2 d\zeta U^2 V}{(c+\zeta)^3} - \frac{c^2 \delta \Delta V \zeta U}{\xi(c+\zeta)^2} - \frac{2c^2 \delta \zeta \nabla U \nabla V}{\xi(c+\zeta)^2} \\ & - \frac{\beta c^2 \delta \Delta U V}{(c+\zeta)^2} - \frac{d\zeta^2 U^2}{(c+\zeta)^2}, \end{aligned} \quad (4.19)$$

and

$$\begin{aligned} \mathcal{H}^V[\mathbf{U}] = & \frac{dU^2 \zeta^2}{(c+\zeta)^2} + \frac{2ac^3 dUV^2 \beta(c-2\zeta)}{(c+\zeta)^3 \xi} + \frac{2c^2 dU^2 V \zeta^2}{(c+\zeta)^3 \xi} \\ & + \frac{2c^4 V^3 \beta(-c+\zeta)}{(c+\zeta)^3 \xi} + \frac{c^3 V^2(c-2\zeta)}{(c+\zeta)^2 \xi} + \frac{4ac^2 dUV \zeta}{(c+\zeta)^2 \xi}, \end{aligned} \quad (4.20)$$

with $\delta = D_2 - D_1$.

At this point, the diffusion coefficient D_2 can be expanded around the critical threshold D_2^c in terms of a small parameter η

$$D_2 = D_2^c + \eta D_2^1 + \eta^2 D_2^2 + \eta^3 D_2^3 + O(\eta^3); \quad (4.21)$$

analogously, we expand also the solution vector \mathbf{U} in terms of η as in (3.24) and rely on the multiple time scale by means of (3.25). When substituting the expansions (3.24)–(3.25) into system (4.18) and collecting terms of the same order in η , we get a set of equations analogous to (3.26)–(3.30).

In detail, at order η , we obtain the equation

$$\mathcal{L}_c \left[\begin{pmatrix} U_1 \\ V_1 \end{pmatrix} \right] = \begin{pmatrix} \mathcal{L}_c^U[U_1, V_1] \\ \mathcal{L}_c^V[U_1, V_1] \end{pmatrix} = 0, \quad (4.22)$$

where \mathcal{L}_c has entries

$$\mathcal{L}_c^U[U_1, V_1] = -\frac{c^2 \delta^c \Delta V_1}{ad(c+\zeta)} - \frac{c V_1 (c + acd - ad\zeta)}{ad(c+\zeta)} + \Delta U_1 \left(D_2^c - \frac{\delta^c \zeta}{c+\zeta} \right) - \frac{U_1 \zeta (a + 2\xi)}{a(c+\zeta)}, \quad (4.23)$$

$$\mathcal{L}_c^V[U_1, V_1] = D_Z \Delta V_1 + \frac{c V_1 (c - \zeta)}{c+\zeta} + \frac{2ad U_1 \zeta}{c+\zeta}, \quad (4.24)$$

with $\delta_c = D_2^c - D_1$. By solving the equation, we can write the solution in the form (3.32) with

$$\rho = \frac{c(c(-ad + \delta^c k_c^2 - 1) + ad\zeta)}{ad(k_c^2(cD_2^c + \zeta(D_2^c - \delta^c)) + \zeta) + 2d\zeta\xi}.$$

At order η^2 , we obtain again

$$\mathcal{L}_c \left[\begin{pmatrix} U_2 \\ V_2 \end{pmatrix} \right] = \frac{\partial}{\partial T_1} \begin{pmatrix} U_1 \\ V_1 \end{pmatrix} - \mathcal{H}_2 \left[\begin{pmatrix} U_1 \\ V_1 \end{pmatrix} \right], \quad \mathcal{H}_2 \left[\begin{pmatrix} U_1 \\ V_1 \end{pmatrix} \right] = \begin{pmatrix} \mathcal{H}_2^U[U_1, V_1] \\ \mathcal{H}_2^V[U_1, V_1] \end{pmatrix}, \quad (4.25)$$

and the components of operator $\mathcal{H}_2[U_1, V_1]$ are given in (A.1) and (A.2). Also in this case, we apply the solvability condition, being the eigenvectors of \mathcal{L}_c^+ of the form (3.34), with

$$\sigma = \frac{c(c(-ad + \delta^c k_c^2 - 1) + ad\zeta)}{ad(-c^2 + c(D_Z k_c^2 + \zeta) + D_Z \zeta k_c^2)}.$$

The condition provides and expression analogous to (3.36), that we omit for brevity. Afterward, we can write again the solution of (4.25) in the form (3.37), where the coefficients are given explicitly in the appendix A.

At order η^3 , in the equation

$$\begin{aligned} \mathcal{L}_c \left[\begin{pmatrix} U_3 \\ V_3 \end{pmatrix} \right] &= \frac{\partial}{\partial T_1} \begin{pmatrix} U_2 \\ V_2 \end{pmatrix} + \frac{\partial}{\partial T_2} \begin{pmatrix} U_1 \\ V_1 \end{pmatrix} - \mathcal{H}_3 \left[\begin{pmatrix} U_1 \\ V_1 \end{pmatrix}, \begin{pmatrix} U_2 \\ V_2 \end{pmatrix} \right], \\ \mathcal{H}_3 \left[\begin{pmatrix} U_1 \\ V_1 \end{pmatrix}, \begin{pmatrix} U_2 \\ V_2 \end{pmatrix} \right] &= \begin{pmatrix} \mathcal{H}_3^U[U_1, V_1, U_2, V_2] \\ \mathcal{H}_3^V[U_1, V_1, U_2, V_2] \end{pmatrix}, \end{aligned} \quad (4.26)$$

the operator $\mathcal{H}_3[U_1, V_1, U_2, V_2]$, whose components are given in (A.5) and (A.6), intervenes; applying again the solvability condition to such equation, we obtain an expression analogous to (3.40), that we omit for brevity.

Finally, following the technique outlined in the previous section, we are able to recover the equations for the amplitudes

$$r_0 \frac{\partial A_j^U}{\partial t} = \mu A_j^U + (s_1 + \mu \tilde{s}_1) \overline{A_l^U} \overline{A_m^U} + A_j^U [s_2 |A_j^U|^2 + s_3 (|A_l^U|^2 + |A_m^U|^2)], \quad (4.27)$$

where

$$r_0 = \frac{ad(c + \zeta)(\rho + \sigma)}{cD_2^c k_c^2 (c - ad\rho)}, \quad \mu = \frac{D_2 - D_2^c}{D_2^c},$$

and $s_1, \tilde{s}_1, s_2, s_3$ are given in (A.7).

As above, we can discuss the emergence and stability of patterns in terms of microscopic quantities; more precisely, in this case, we fix some parameters as in (4.17) and let E_2 and $\bar{\nu}_B$ vary. In Figure 7, different regions are individuated, according to the stability of the pattern: we obtain striped patterns in region I, hexagons in region III, and the coexistence of both in region II. We highlight that no patterns are expected to exist and to be stable in region IV. Results are summarized in Table 3.

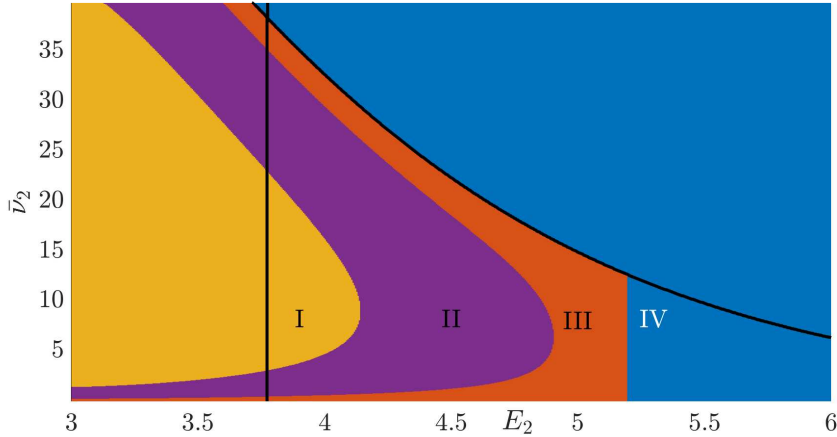


Figure 7: Values for energy level E_2 and collision frequency $\bar{\nu}_2$ relevant to the stability of the different patterns for system (2.20). Black lines define the region where Turing instability can occur, leading to stable striped patterns (region I), coexistence of stable striped and hexagonal pattern (region II), stable hexagonal pattern (region III) or to stable pattern-less configuration (region IV). Parameters are chosen as in (3.17).

Table 3: Classification of steady states in cross diffusion model (stripes \mathcal{S} , hexagons $\mathcal{H}_l^\pm, l = 0, \pi$) in each region of Figure 7.

Region	Stable Equilibria
I	\mathcal{S}
II	$\mathcal{S}, \mathcal{H}_\pi^\pm$
III	\mathcal{H}_π^-
IV	—

4.2 Numerical simulations

The theoretical results obtained in the previous subsection can be confirmed by means of numerical simulations for system (2.20) by taking E_2 $\bar{\nu}_2$ in the different regions of Figure 7; the corresponding coefficients of the macroscopic system (2.20) are reported in Table 4. All the remaining microscopic parameters are set as in (4.17). In this case, numerical simulations are performed on a two-dimensional square domain of length $L = 10\pi$, discretized into a 250×250 grid, starting from a perturbation of the homogeneous equilibrium shaped as cosines in the three directions \mathbf{k}_i , up to final time $t = 500$.

Case 1. As first case, we take values of E_2 and $\bar{\nu}_2$ in region I (more precisely $E_2 = 4.04$ and $\bar{\nu}_2 = 13.24$). As predicted by the analysis, this choice leads to stable striped pattern, as shown in Figure 8.

Case 2. As second test, we consider E_2 and $\bar{\nu}_2$ in region II ($E_2 = 4.04$ and $\bar{\nu}_2 = 23.19$). As shown, these values correspond to the coexistence of stable hexagons (with phase angle $\phi = \pi$) and striped patterns, as shown in Figure 9.

Table 4: Values of coefficients for macroscopic system (2.20) taking microscopic values as in (4.17), for different choices of E_2 and $\bar{\nu}_2$.

Case	E_2	$\bar{\nu}_2$	a	β	c	d	D_1	D_2	D_Z	Region
1	4.04	13.34	2.5	0.11	40	20	1	6	2	I
2	4.45	13.34	2.5	0.15	40	20	1	6	2	II
3	4.98	13.34	2.5	0.23	40	20	1	6	2	III

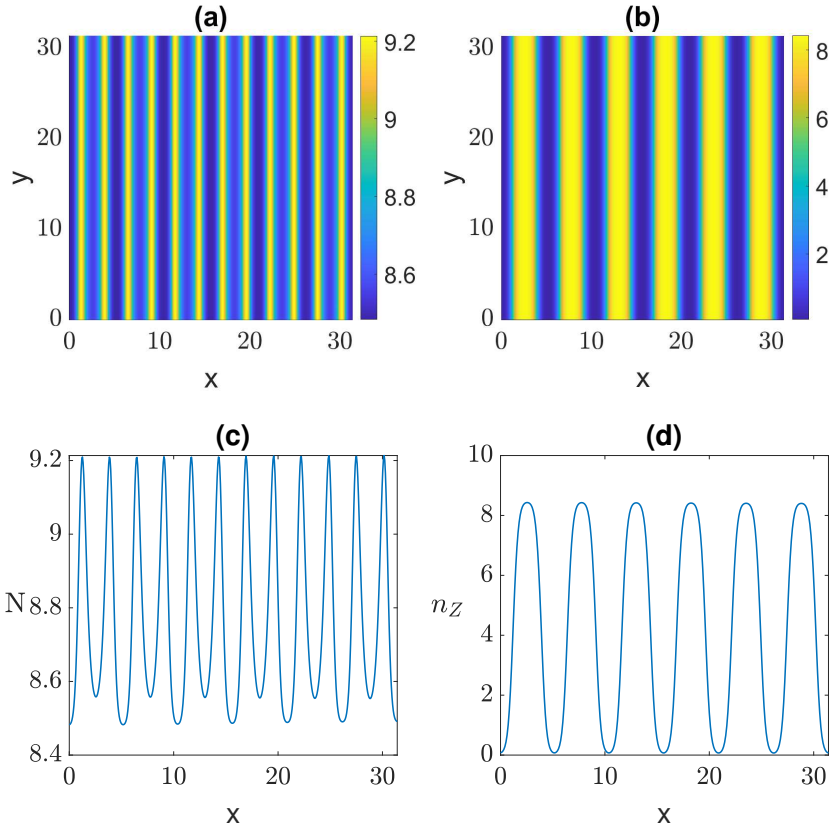


Figure 8: Pattern formation for system (2.20) in a squared domain Ω assuming no-flux conditions at the boundary $\partial\Omega$, and taking coefficient as reported in the first row of Table 4. Panel (a): density of N . Panel (b): density of n_Z . Panel (c): section of density of N at $y = 15$. Panel (d): section of density of n_Z at $y = 15$.

Case 3. Finally, we choose $E_2 = 4.98$ and $\bar{\nu}_2 = 13.34$, i.e. in region III. The emergence of stable hexagons corresponding (with phase angle $\phi = \pi$) is confirmed, as shown in Figure 10.

Although some patterns presented here may resemble those reported in other contexts, it is worth underlying that the results shown are entirely new; as already noted, the proposed model reproduces the diffusive mechanism of [13], but its reactive terms are

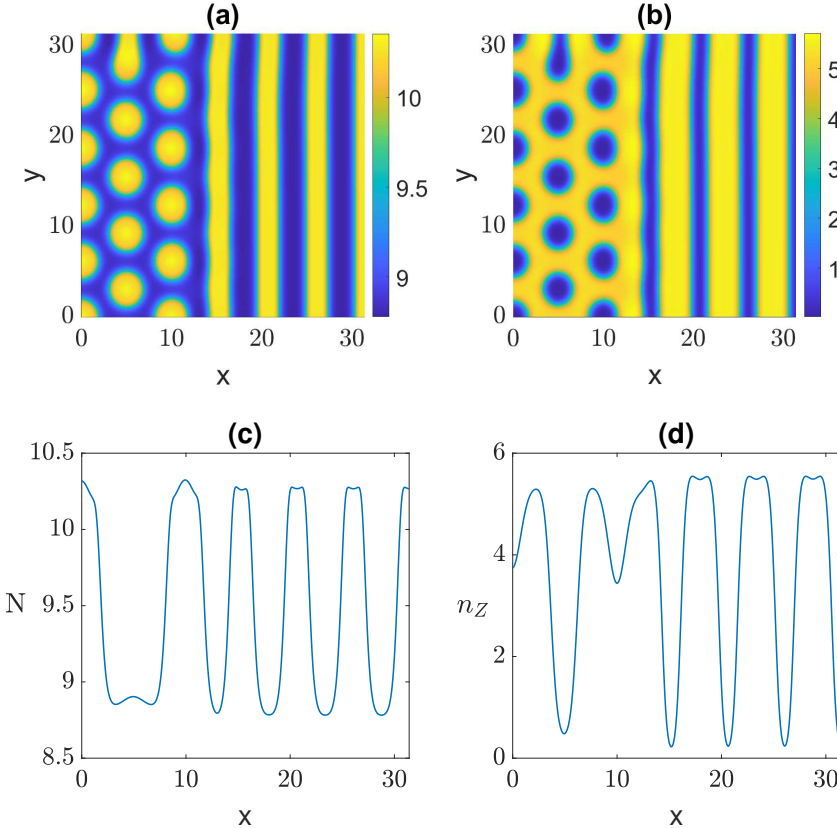


Figure 9: Pattern formation for system (2.20) in a squared domain Ω assuming no-flux conditions at the boundary $\partial\Omega$, and taking coefficient as reported in the second row of Table 4. Panel (a): density of N . Panel (b): density of n_Z . Panel (c): section of density of N at $y = 15$. Panel (d): section of density of n_Z at $y = 15$.

substantially different.

Moreover, we point out that, as shown also in the one-dimensional case in [27], the numerical results suggest that the profile of N is sum of more than one mode in each direction \mathbf{k}_i . Therefore, a deeper analysis of the solution near the critical threshold is needed; this will be subject of future investigation.

5 Conclusions

In this paper, we have discussed Turing instability and pattern formation in two-dimensional domains for two reaction-diffusion models for gas mixtures of monatomic and polyatomic components, obtained as diffusive limits of kinetic equations. The derivation from the mesoscopic level offers the significant advantage of relating macroscopic coefficients, usually set empirically, to microscopic parameters, and therefore to the mechanisms of interaction

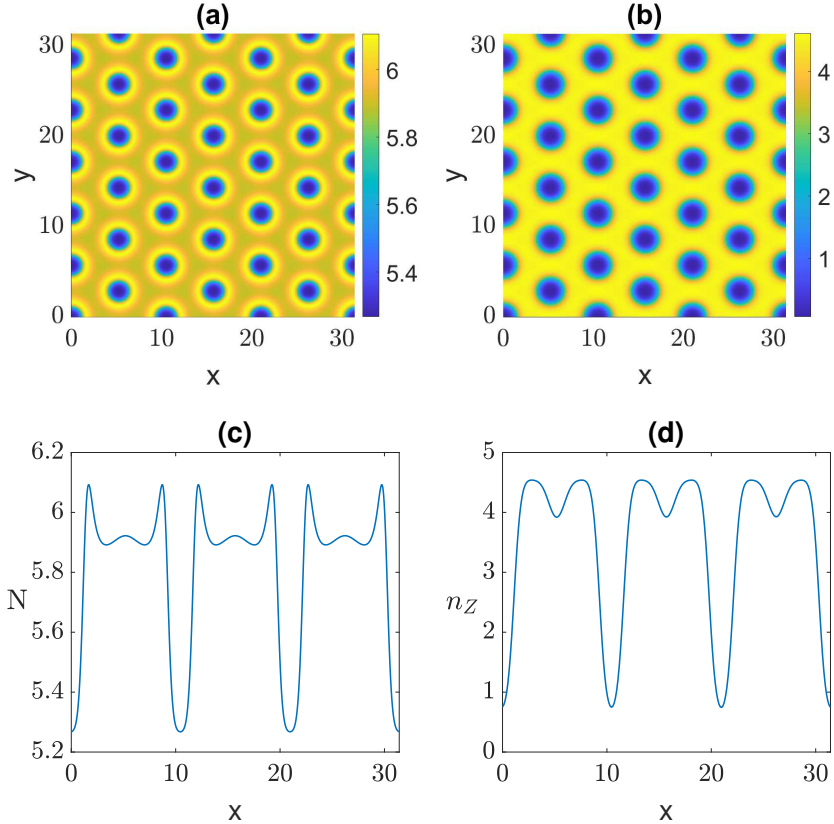


Figure 10: Pattern formation for system (2.20) in a squared domain Ω assuming no-flux conditions at the boundary $\partial\Omega$, and taking coefficient as reported in the third row of Table 4. Panel (a): density of N . Panel (b): density of n_Z . Panel (c): section of density of N at $y = 15$. Panel (d): section of density of n_Z at $y = 15$.

among the components or with the environment. This connection also rigorously identifies suitable ranges for selecting the macroscopic parameters.

In the first model under consideration, we showed how the kinetic derivation of Brusselator-type equations reveals the presence of an additional parameter d , which is typically set equal to 1 in the literature. The presence of this parameter has several effects, as it influences, for instance, the equilibria and their stability. With respect to pattern formation, d does not affect the variety of patterns that may emerge (which remain the same as in the case $d = 1$), but it does affect their amplitude.

In the second framework analyzed, the resulting model exhibits nonlinear cross-diffusion terms, as in [13], though with different reactive terms. Pattern formation is investigated theoretically through weakly nonlinear analysis and confirmed numerically, thereby extending the preliminary results obtained in the one-dimensional case in [27].

The proposed analysis shows the strength of these tools in linking macroscopic dynamics to microscopic interaction mechanisms. These, along with other approaches (such as active

particle theory or redistribution operators), allow one to derive, and thus mathematically justify, several models already known in the literature, while providing broader insight into their behavior. In this perspective, future work will be devoted to the derivation of alternative reactive terms, such as those proposed in [13]. A careful calibration of these terms, based also on a deep knowledge of the underlying microscopic interaction mechanisms, is essential, as the intrinsic nonlinearities in them play a crucial role in enhancing the realism of the models. These nonlinear effects not only allow a more faithful representation of the processes but also provide the key element to reproducing and interpreting the rich variety of spatial patterns observed in real systems.

Finally, as argued above, further attention will be devoted to analyze the behavior of the densities and the possible presence of interacting modes whose study is particularly useful in applications because the coupling among spatial modes can lead to the emergence of complex patterns, influence their stability, and affect their shape. Understanding these interactions could help to better clarify the mechanisms behind complex structures observed in real ecosystems, such as mixed and oscillating patterns, and to interpret empirical data and evidence. In addition, in this work, we have focused on the patterns predicted analytically near the critical thresholds, showing that stable spatial structures emerge from perturbations of the equilibrium. More complex and temporally oscillating patterns may arise from initial conditions far from these thresholds [7], and we plan to investigate these richer dynamics in future work.

Acknowledgments This work was performed in the frame of activities sponsored by the Italian National Group of Mathematical Physics (GNFM-INDAM) and by the Universities of Parma (Italy) and Pavia (Italy). RT has been supported by the National Institute of Advanced Mathematics (INDAM), Italy. RT also thanks the support of the University of Parma through the action Bando di Ateneo 2022 per la ricerca, cofunded by MUR-Italian Ministry of Universities and Research - D.M. 737/2021 - PNR - PNRR - NextGenerationEU (project "Collective and Self-Organised Dynamics: Kinetic and Network Approaches"). The work of SB was supported by an appointment to the NASA Postdoctoral Program, held at NASA Goddard Space Flight Center and administered by Oak Ridge Associated Universities.

A Weakly nonlinear analysis in cross diffusion model

- Components of operator $\mathcal{H}_2[U_1, V_1]$ in (4.25)

$$\begin{aligned}\mathcal{H}_2^U[U_1, V_1] = & \frac{c^3 V_1^2 (a\beta - c + 2\zeta)}{\xi(c + \zeta)^2} + \frac{2a\beta c^3 \delta^c \Delta V_1 V_1}{\xi(c + \zeta)^2} + \frac{2a\beta c^3 \delta^c \nabla V_1 \cdot \nabla V_1}{\xi(c + \zeta)^2} \\ & - \frac{c^2 \zeta U_1 V_1 (4ad + 1)}{\xi(c + \zeta)^2} - \frac{ac^2 D_2^1 \Delta V_1}{\xi(c + \zeta)} - \frac{c^2 \delta^c \Delta V_1 \zeta U_1}{\xi(c + \zeta)^2} \\ & - \frac{2c^2 \delta^c \zeta \nabla U_1 \cdot \nabla V_1}{\xi(c + \zeta)^2} - \frac{c^2 \delta^c \Delta U_1 \zeta V_1}{\xi(c + \zeta)^2} - \frac{d\zeta^2 U_1^2}{(c + \zeta)^2} + \frac{c D_2^1 \Delta U_1}{c + \zeta},\end{aligned}\tag{A.1}$$

$$\mathcal{H}_2^V[U_1, V_1] = \frac{4ac^2 d\zeta U_1 V_1}{\xi(c + \zeta)^2} + \frac{c^3 V_1^2 (c - 2\zeta)}{\xi(c + \zeta)^2} + \frac{d\zeta^2 U_1^2}{(c + \zeta)^2}.\tag{A.2}$$

- Coefficients of the solution of (4.25) in the form (3.37)

$$X_0 = \frac{2c(c^2(-c^2 + c\zeta + \zeta^2) - acd\zeta(3c + \zeta)\rho - d\zeta^2\xi\rho^2)}{ad\zeta(c + \zeta)^2\xi}, \quad Y_0 = \frac{2(c^2 + ad\zeta\rho)^2}{c(c + \zeta)^2\xi},$$

$$\begin{aligned}X_1 = & - \left[2c^2 d\zeta \rho \left(a(3\delta^c k_c^2 - 1) (\zeta(c + 3D_Z k_c^2) + 3c(c + D_Z k_c^2)) - 12D_Z k_c^2 \xi(c + \zeta) \right) \right. \\ & + 2c^3 \left(c^2 (\zeta - 3k_c^2(adD_Z + \delta^c\zeta)) + c\zeta (3k_c^2(adD_Z - \delta^c\zeta - 3\delta^c D_Z k_c^2 + D_Z) + \zeta) \right. \\ & \left. \left. + 3D_Z \zeta^2 k_c^2 (2ad - 3\delta^c k_c^2 + 1) + c^3 (3\delta^c k_c^2 - 1) \right) \right. \\ & \left. - 2d\zeta^2 \xi \rho^2 (c(3adD_Z k_c^2 - 3c\delta^c k_c^2 + c) + 3adD_Z \zeta k_c^2) \right] \\ & \times \left[d\xi(c + \zeta)^2 \left(-a\zeta(c + 3D_Z k_c^2) (3k_c^2(D_2^c - \delta^c) + 1) + 3ac D_2^c k_c^2 (c - 3D_Z k_c^2) - 6D_Z \zeta k_c^2 \xi \right) \right]^{-1},\end{aligned}\tag{A.3}$$

$$\begin{aligned}
Y_1 &= \left[4ac^2 d\zeta \rho \left(3k_c^2 (2cD_2^c + 2D_2^c \zeta - \delta^c \zeta) + \zeta \right) + 2c^3 \left(3c^2 D_2^c k_c^2 + c\zeta (1 - 3k_c^2 (D_2^c + \delta^c)) - 6D_2^c \zeta^2 k_c^2 \right) \right. \\
&\quad \left. + 2d\zeta^2 \xi \rho^2 \left(3k_c^2 (cD_2^c + \zeta (D_2^c - \delta^c)) + \zeta \right) \right] \\
&\quad \times \left[a^2 d(c + \zeta)^2 \left(\zeta \left(3D_Z k_c^2 (2ad + 3k_c^2 (D_2^c - \delta^c) + 1) + 3ck_c^2 (D_2^c - \delta^c) + c \right) \right. \right. \\
&\quad \left. \left. - 3cD_2^c k_c^2 (c - 3D_Z k_c^2) \right) \right]^{-1}, \\
X_2 &= - \left[c^2 d\zeta \rho \left(a(4\delta^c k_c^2 - 1) (3c^2 + c(4D_Z k_c^2 + \zeta) + 4D_Z \zeta k_c^2) - 16D_Z k_c^2 \xi (c + \zeta) \right) \right. \\
&\quad + c^3 \left(c^2 (\zeta - 4k_c^2 (adD_Z + \delta^c \zeta)) + c\zeta (4D_Z k_c^2 (ad - 4\delta^c k_c^2 + 1) + \zeta - 4\delta^c \zeta k_c^2) \right. \\
&\quad \left. + 4D_Z \zeta^2 k_c^2 (2ad - 4\delta^c k_c^2 + 1) + c^3 (4\delta^c k_c^2 - 1) \right) \\
&\quad \left. - d\zeta^2 \xi \rho^2 (c(4adD_Z k_c^2 - 4c\delta^c k_c^2 + c) + 4adD_Z \zeta k_c^2) \right] \\
&\quad \times \left[d\xi (c + \zeta)^2 \left(-a\zeta (c + 4D_Z k_c^2) (4k_c^2 (D_2^c - \delta^c) + 1) + 4acD_2^c k_c^2 (c - 4D_Z k_c^2) - 8D_Z \zeta k_c^2 \xi \right) \right]^{-1}, \\
Y_2 &= \left[2ac^2 d\zeta \rho \left(4k_c^2 (2cD_2^c + 2D_2^c \zeta - \delta^c \zeta) + \zeta \right) + c^3 \left(4c^2 D_2^c k_c^2 + c\zeta (1 - 4k_c^2 (D_2^c + \delta^c)) - 8D_2^c \zeta^2 k_c^2 \right) \right. \\
&\quad \left. + d\zeta^2 \xi \rho^2 \left(4k_c^2 (cD_2^c + \zeta (D_2^c - \delta^c)) + \zeta \right) \right] \\
&\quad \times \left[a^2 d(c + \zeta)^2 \left(\zeta \left(4D_Z k_c^2 (2ad + 4k_c^2 (D_2^c - \delta^c) + 1) + 4ck_c^2 (D_2^c - \delta^c) + c \right) \right. \right. \\
&\quad \left. \left. - 4cD_2^c k_c^2 (c - 4D_Z k_c^2) \right) \right]^{-1}. \tag{A.4}
\end{aligned}$$

- Components of operator $\mathcal{H}_3 [U_1, V_1, U_2, V_2]$ in (4.26)

$$\begin{aligned}
\mathcal{H}_3^U(U_1, V_1, U_2, V_2) = & \frac{\beta c^4 V_1^3 (-a\beta + 2c - 2\zeta)}{\xi(c + \zeta)^3} - \frac{3a\beta^2 c^4 \delta^c \Delta V_1 V_1^2}{\xi(c + \zeta)^3} - \frac{6a\beta^2 c^4 \delta^c V_1 \nabla V_1 \cdot \nabla V_1}{\xi(c + \zeta)^3} \\
& + \frac{\beta c^3 U_1 V_1^2 (\zeta - 2ad(c - 2\zeta))}{\xi(c + \zeta)^3} + \frac{2a\beta c^3 D_2^1 \Delta V_1 V_1}{\xi(c + \zeta)^2} + \frac{2a\beta c^3 D_2^1 \nabla V_1 \cdot \nabla V_1}{\xi(c + \zeta)^2} \\
& + \frac{2a\beta c^3 \delta^c \Delta V_2 V_1}{\xi(c + \zeta)^2} + \frac{4a\beta c^3 \delta^c \nabla V_1 \nabla V_2}{\xi(c + \zeta)^2} + \frac{2c^3 V_1 V_2 (a\beta - c + 2\zeta)}{\xi(c + \zeta)^2} \\
& + \frac{2a\beta c^3 \delta^c \Delta V_1 V_2}{\xi(c + \zeta)^2} - \frac{c^2 \zeta U_1 V_2 (4ad + 1)}{\xi(c + \zeta)^2} - \frac{c^2 \zeta U_2 V_1 (4ad + 1)}{\xi(c + \zeta)^2} - \frac{ac^2 D_2^1 \Delta V_2}{\xi(c + \zeta)} \\
& + \frac{2\beta c^3 \delta^c \zeta U_1 V_1 \Delta V_1}{\xi(c + \zeta)^3} + \frac{2\beta c^3 \delta^c \zeta U_1 \nabla V_1 \cdot \nabla V_1}{\xi(c + \zeta)^3} + \frac{4\beta c^3 \delta^c \zeta V_1 \nabla U_1 \cdot \nabla V_1}{\xi(c + \zeta)^3} \\
& + \frac{\beta c^3 \delta^c \zeta V_1^2 \Delta U_1}{\xi(c + \zeta)^3} - \frac{2c^2 d \zeta^2 U_1^2 V_1}{\xi(c + \zeta)^3} - \frac{c^2 D_2^1 \zeta U_1 \Delta V_1}{\xi(c + \zeta)^2} - \frac{ac^2 D_2^2 \Delta V_1}{\xi(c + \zeta)} \\
& - \frac{2c^2 D_2^1 \zeta \nabla U_1 \cdot \nabla V_1}{\xi(c + \zeta)^2} - \frac{c^2 D_2^1 \zeta V_1 \Delta U_1}{\xi(c + \zeta)^2} - \frac{c^2 \delta^c \zeta U_1 \Delta V_2}{\xi(c + \zeta)^2} \\
& - \frac{2c^2 \delta^c \zeta \nabla U_1 \cdot \nabla V_2}{\xi(c + \zeta)^2} - \frac{c^2 \delta^c \zeta U_2 \Delta V_1}{\xi(c + \zeta)^2} - \frac{2c^2 \delta^c \zeta \nabla U_2 \cdot \nabla V_1}{\xi(c + \zeta)^2} \\
& - \frac{c^2 \delta^c \zeta V_1 \Delta U_2}{\xi(c + \zeta)^2} - \frac{c^2 \delta^c \zeta V_2 \Delta U_1}{\xi(c + \zeta)^2} - \frac{2d \zeta^2 U_1 U_2}{(c + \zeta)^2} + \frac{c D_2^1 \Delta U_2}{c + \zeta} + \frac{c D_2^2 \Delta U_1}{c + \zeta}, \tag{A.5}
\end{aligned}$$

$$\begin{aligned}
\mathcal{H}_3^V(U_1, V_1, U_2, V_2) = & \frac{2a\beta c^3 d U_1 V_1^2 (c - 2\zeta)}{\xi(c + \zeta)^3} + \frac{4ac^2 d \zeta U_1 V_2}{\xi(c + \zeta)^2} + \frac{4ac^2 d \zeta U_2 V_1}{\xi(c + \zeta)^2} \tag{A.6} \\
& + \frac{2\beta c^4 V_1^3 (\zeta - c)}{\xi(c + \zeta)^3} + \frac{2c^3 V_1 V_2 (c - 2\zeta)}{\xi(c + \zeta)^2} + \frac{2c^2 d \zeta^2 U_1^2 V_1}{\xi(c + \zeta)^3} + \frac{2d \zeta^2 U_1 U_2}{(c + \zeta)^2}.
\end{aligned}$$

- Coefficients of system (4.27)

$$\begin{aligned}
s_1 &= \frac{2\tau \left(4ac^2 d\zeta \rho + c^4 - 2c^3 \zeta + d\zeta^2 \xi \rho^2 \right) - 2c^2 (\delta^c k_c^2 - 1) (a\beta c - \zeta \rho)}{c D_2^c k_c^2 \rho^2 (c + \zeta) (ac - \xi \rho)}, \quad \tilde{s}_1 = -\frac{2\beta c}{\rho^2 (c + \zeta)}, \\
s_2 &= \left\{ ac^2 \left[\beta c^2 \left(-3\beta + 6d\rho\tau + \delta^c k_c^2 (3\beta - 2(Y_0 + 5Y_2)) + 2Y_0 + 2Y_2 \right) \right. \right. \\
&\quad - 2c\zeta \left(6\beta d\rho\tau - 2d\tau (X_0 + X_2 + \rho(Y_0 + Y_2)) + \beta \delta^c k_c^2 (Y_0 + 5Y_2) - \beta (Y_0 + Y_2) \right) \\
&\quad \left. \left. + 4d\zeta^2 \tau (X_0 + X_2 + \rho(Y_0 + Y_2)) \right] + 2c^5 \tau (-3\beta + Y_0 + Y_2) - 2c^4 \zeta \tau (-3\beta + Y_0 + Y_2) \right. \\
&\quad + c^3 \zeta \left(X_0 (\delta^c k_c^2 - 1) + X_2 (5\delta^c k_c^2 - 1) + \rho (\delta^c k_c^2 - 1) (-3\beta + Y_0 + Y_2) - 4\zeta \tau (Y_0 + Y_2) \right) \\
&\quad + c^2 \zeta^2 \left(6d\rho^2 \tau + \delta^c k_c^2 (X_0 + 5X_2 + \rho(Y_0 + Y_2)) - X_0 - X_2 - \rho(Y_0 + Y_2) \right) \\
&\quad \left. \left. + 2cd\zeta^2 \xi \rho \tau (X_0 + X_2) + 2d\zeta^3 \xi \rho \tau (X_0 + X_2) \right\} [c D_2^c k_c^2 \rho^3 (c + \zeta)^2 (ac - \xi \rho)]^{-1}, \right. \\
s_3 &= \left\{ 2ac^2 \left[-\beta c^2 \left(-3\beta + 6d\rho\tau - \delta^c k_c^2 (-3\beta + Y_0 + 4Y_1) + Y_0 + Y_1 \right) \right. \right. \\
&\quad + c\zeta \left(12\beta d\rho\tau - 2d\tau (X_0 + X_1 + \rho(Y_0 + Y_1)) + \beta \delta^c k_c^2 (Y_0 + 4Y_1) - \beta (Y_0 + Y_1) \right) \\
&\quad \left. \left. - 2d\zeta^2 \tau (X_0 + X_1 + \rho(Y_0 + Y_1)) \right] - 2c^5 \tau (-6\beta + Y_0 + Y_1) + 2c^4 \zeta \tau (-6\beta + Y_0 + Y_1) \right. \\
&\quad - c^3 \zeta \left(X_0 (\delta^c k_c^2 - 1) + X_1 (4\delta^c k_c^2 - 1) + \rho (\delta^c k_c^2 - 1) (-6\beta + Y_0 + Y_1) - 4\zeta \tau (Y_0 + Y_1) \right) \\
&\quad - c^2 \zeta^2 \left(12d\rho^2 \tau + \delta^c k_c^2 (X_0 + 4X_1 + \rho(Y_0 + Y_1)) - X_0 - X_1 - \rho(Y_0 + Y_1) \right) \\
&\quad \left. \left. - 2cd\zeta^2 \xi \rho \tau (X_0 + X_1) - 2d\zeta^3 \xi \rho \tau (X_0 + X_1) \right\} [-c D_2^c k_c^2 \rho^3 (c + \zeta)^2 (ac - \xi \rho)]^{-1}, \right. \\
&\quad \text{with } \tau = 1 - \sigma.
\end{aligned} \tag{A.7}$$

References

- [1] M. Abbas, F. Giannino, A. Iuorio, Z. Ahmad, and F. Calabrò. PDE models for vegetation biomass and autotoxicity. *Math. Comput. Simul.*, 228:386–401, 2025.
- [2] M. Banerjee, S. Ghosh, P. Manfredi, and A. d’Onofrio. Spatio-temporal chaos and clustering induced by nonlocal information and vaccine hesitancy in the SIR epidemic model. *Chaos Solit. Fractals*, 170:113339, 2023.
- [3] M. Banerjee, S. V. Petrovskii, and V. Volpert. Nonlocal reaction–diffusion models of heterogeneous wealth distribution. *Mathematics*, 9(4):351, 2021.
- [4] N. Bellomo, L. Gibelli, A. Quaini, and A. Reali. Towards a mathematical theory of behavioral human crowds. *Math. Models Methods Appl. Sci.*, 32(02):321–358, 2022.

- [5] M. Bisi and L. Desvillettes. From reactive boltzmann equations to reaction–diffusion systems. *J. Stat. Phys.*, 124(2):881–912, 2006.
- [6] M. Bisi, M. Groppi, G. Martalò, and C. Soresina. A chemotaxis reaction–diffusion model for Multiple Sclerosis with Allee effect. *Ric. Mat.*, 73(Suppl 1):29–46, 2024.
- [7] M. Bisi, M. Groppi, G. Martalò, and R. Travaglini. Derivation from kinetic theory and 2-D pattern analysis of chemotaxis models for Multiple Sclerosis. *J. Math. Biol.*, 91(43), 2025.
- [8] M. Bisi and R. Travaglini. Reaction-diffusion equations derived from kinetic models and their Turing instability. *Commun. Math. Sci.*, 20(3):763–801, 2022.
- [9] S. Boccelli. Hyper2d: A finite-volume solver for hyperbolic equations and non-equilibrium flows. *Softw. Impacts*, 17:100557, 2023.
- [10] A. Bondesan, M. Menale, G. Toscani, and M. Zanella. Lotka–Volterra-type kinetic equations for interacting species. *Nonlinearity*, 38(7):075026, 2025.
- [11] D. Burini and N. Chouhad. A multiscale view of nonlinear diffusion in biology: From cells to tissues. *Math. Models Methods Appl. Sci.*, 29(04):791–823, 2019.
- [12] C. Cercignani. The boltzmann equation. In *The Boltzmann equation and its applications*, pages 40–103. Springer, 1988.
- [13] F. Conforto, L. Desvillettes, and C. Soresina. About reaction–diffusion systems involving the Holling-type II and the Beddington–DeAngelis functional responses for predator–prey models. *NoDEA*, 25(3):24, 2018.
- [14] G. Consolo, C. Currò, G. Grifò, and G. Valenti. Vegetation pattern formation and transition in dryland ecosystems with finite soil resources and inertia. *Phys. D: Nonlinear Phenom.*, 476:134601, 2025.
- [15] R. Della Marca, A. d’Onofrio, C. F. Munafò, and R. Travaglini. Spatiotemporal quasiperiodicity induced by all–ages vaccine hesitancy in an sir model. *Phys. D: Nonlinear Phenom.*, page 135010, 2025.
- [16] G. Gambino, M. C. Lombardo, and V. Sciacca. Turing pattern formation in the Brusselator system with nonlinear diffusion. *Phys. Rev. E*, 88(4):042925, 2013.
- [17] F. Gargano, M. C. Lombardo, R. Rizzo, M. Sammartino, and V. Sciacca. Cytokine-induced instabilities in a reaction–diffusion-chemotaxis model of Multiple Sclerosis: Bifurcation analysis and well-posedness. *Int. J. Non-Linear Mech.*, 161:104672, 2024.
- [18] V. Giovangigli. Multicomponent flow modeling. *Sci. China Math.*, 55(2):285–308, 2012.

- [19] M. Groppi and G. Spiga. Kinetic approach to chemical reactions and inelastic transitions in a rarefied gas. *J. Math. Chem.*, 26(1):197–219, 1999.
- [20] S. L. Judd and M. Silber. Simple and superlattice turing patterns in reaction–diffusion systems: bifurcation, bistability, and parameter collapse. *Phys. D: Nonlinear Phenom.*, 136(1-2):45–65, 2000.
- [21] M. Lachowicz. From microscopic to macroscopic description for generalized kinetic models. *Math. Models Methods Appl. Sci.*, 12(07):985–1005, 2002.
- [22] R. Lefever, G. Nicolis, and P. Borckmans. The brusselator: it does oscillate all the same. *J. Chem. Soc. Faraday Trans.*, 84(4):1013–1023, 1988.
- [23] I. Lengyel and I. R. Epstein. Modeling of turing structures in the chlorite–iodide–malonic acid–starch reaction system. *Science*, 251(4994):650–652, 1991.
- [24] X. Li, G. Hu, and Z. Feng. Pattern dynamics in a spatial predator–prey model with nonmonotonic response function. *Int J Bifurc Chaos*, 28(06):1850077, 2018.
- [25] T. T. Marquez-Lago and P. Padilla. A selection criterion for patterns in reaction–diffusion systems. *Theor. Biol. Med. Model.*, 11(1):7, 2014.
- [26] G. Martalò, G. Toscani, and M. Zanella. Individual-Based Foundation of SIR-Type Epidemic Models: mean-field limit and large time behaviour. *arXiv preprint arXiv:2507.13947*, 2025.
- [27] G. Martalò and R. Travaglini. A reaction-cross-diffusion model derived from kinetic equations for gas mixtures. *Phys. D: Nonlinear Phenom.*, 459:134029, 2024.
- [28] G. Mascali and V. Romano. Exploitation of the maximum entropy principle in mathematical modeling of charge transport in semiconductors. *Entropy*, 19(1):36, 2017.
- [29] C. B. Muratov and V. V. Osipov. Scenarios of domain pattern formation in a reaction–diffusion system. *Phys. Rev. E*, 54(5):4860, 1996.
- [30] J. D. Murray. Spatial models and biomedical applications. *Mathematical Biology*, 2003.
- [31] Q. Ouyang. *Pattern Formation in Reaction–Diffusion Systems*. Shanghai Scientific and Technological Education Publishing House, Shanghai, 2000.
- [32] B. Pena and C. Perez-Garcia. Stability of Turing patterns in the Brusselator model. *Phys. Rev. E*, 64(5):056213, 2001.
- [33] I. Prigogine and R. Lefever. Symmetry breaking instabilities in dissipative systems. ii. *J. Chem. Phys.*, 48(4):1695–1700, 1968.

- [34] R. Spigler and D. H. Zanette. Reaction-diffusion models from the fokker-planck formulation of chemical processes. *IMA J. Appl. Math.*, 49(3):217–229, 1992.
- [35] R. Spigler and D. H. Zanette. Asymptotic analysis and reaction-diffusion approximation for bgk kinetic models of chemical processes in multispecies gas mixtures. *Z. fur Angew. Math. Phys.*, 44(5):812–827, 1993.
- [36] R. Spigler and D. H. Zanette. A bgk model for chemical processes: The reaction-diffusion approximation. *Math. Models Methods Appl. Sci.*, 4(01):35–47, 1994.
- [37] H. Struchtrup and A. Frezzotti. Twenty-six moment equations for the enskog–vlasov equation. *J. Fluid Mech.*, 940:A40, 2022.
- [38] A. M. Turing. The chemical basis of morphogenesis. *Bull. Math. Biol.*, 52(1):153–197, 1990.
- [39] J. Verdasca, A. De Wit, G. Dewel, and P. Borckmans. Reentrant hexagonal Turing structures. *Phys. Lett.*, 168(3):194–198, 1992.
- [40] L. Yang, M. Dolnik, A. M. Zhabotinsky, and I. R. Epstein. Turing patterns beyond hexagons and stripes. *Chaos*, 16(3), 2006.
- [41] D. H. Zanette. Linear and nonlinear diffusion and reaction-diffusion equations from discrete-velocity kinetic models. *J. Phys. A: Math. Gen.*, 26(20):5339, 1993.